

Top-Quark Physics at the LHC

Kevin Kröninger[†], Andreas B. Meyer[‡] and Peter Uwer^{II}

[†]Technische Universität Dortmund, Fakultät Physik, Otto-Hahn-Str. 4, 44227 Dortmund, Germany

[‡]Deutsches Elektronen-Synchrotron (DESY), Notkestr. 85, 22607 Hamburg, Germany

^{II}Humboldt-Universität zu Berlin, Institut für Physik, Newtonstraße 15, 12489 Berlin, Germany

Abstract. The top quark is the heaviest of all known elementary particles. It was discovered in 1995 by the CDF and DØ experiments at the Tevatron. With the start of the LHC in 2009, an unprecedented wealth of measurements of the top quark’s production mechanisms and properties have been performed by the ATLAS and CMS collaborations, most of these resulting in smaller uncertainties than those achieved previously. At the same time, huge progress was made on the theoretical side yielding significantly improved predictions up to next-to-next-to-leading order in perturbative QCD. Due to the vast amount of events containing top quarks, a variety of new measurements became feasible and opened a new window to precision tests of the Standard Model and to contributions of new physics. In this review, originally written for a recent book on the results of LHC Run 1 [1], top-quark measurements obtained so far from the LHC Run 1 are summarised and put in context with the current understanding of the Standard Model.

Contents

| | | |
|---|--|----|
| 1 | Introduction | 1 |
| 2 | Top-Quark Pair Production | 2 |
| 3 | Top-Quark Mass | 9 |
| 4 | Tests of QCD Predictions | 14 |
| 5 | Tests of Electroweak Predictions | 20 |
| 6 | Single Top-Quark Production | 22 |
| 7 | Conclusions | 27 |

1 Introduction

Top quarks have been a subject of scientific research ever since Kobayashi’s and Maskawa’s speculations about a third family of quarks in the context of solving the problem of weak CP violation in the early 1970s [2]. After a two-decade long period of searches at various colliders and experiments, the top quark was finally discovered in 1995 by the CDF and DØ experiments at Fermilab’s Tevatron, a proton-antiproton collider, operated at the time at a centre-of-mass energy of $\sqrt{s} = 1.80$ TeV [3, 4]. Since then, and in particular after the upgrade of the Tevatron to a centre-of-mass energy of 1.96 TeV, pioneering precision measurements were performed at this machine. Prime examples are the measurements of the total cross section for single-top and top-quark pair ($t\bar{t}$) production and the measurements of the top-quark mass (see Refs. [5, 6] and references therein). Currently, both CDF and DØ are in the process of publishing their legacy measurements based on data sets corresponding to an integrated luminosity of about 10 fb^{-1} collected by each experiment during Tevatron Run 2—and these measurements set a standard for the LHC.

A new era in experimental top-quark physics was marked by the start of the LHC in 2009. At the LHC, top quarks are produced abundantly due to the high centre-of-mass energy, the resulting large rise of the parton luminosities, and the large instantaneous luminosity of the accelerator. During LHC’s Run 1

Originally published in “The Large Hadron Collider — Harvest of Run 1”, edited by T. Schörner-Sadenius, Springer, 2015, pp. 259–300 [1].

more than 5 million top-quark events were produced at the collision points in ATLAS and CMS each. Based on these huge data samples, most of the measurements performed at the Tevatron have already been improved and/or complementary studies have been performed. This has only been made possible by inheriting a wealth of analysis techniques from the Tevatron experiments where they were pioneered and brought to perfection. At the LHC, top quarks have become tools for searches for new physics, e.g. the search for rare decays, for measurements of top-quark couplings to gauge bosons, or for the investigation of the proton structure.

In this chapter the experimental findings obtained during LHC Run 1 are summarised and put in context with our current understanding of the Standard Model (SM). Emphasis is placed on three aspects: i) the description of the precision measurements in comparison with results from the Tevatron and with theory predictions, e.g. production cross sections or top-quark properties; ii) the presentation of new measurements that were not performed at the Tevatron and that either improve the current understanding of already measured quantities or enable measurements of yet unexplored processes and quantities, e.g. small couplings or associated production processes; iii) the discussion of the physics lessons and insights gained from the LHC Run 1 results. These results do not only impact on our understanding of the Standard Model, but also help us prepare for future investigations at the LHC and beyond. Several important measurements based on the data from LHC Run 1 are still being performed. This chapter can thus not be complete, and only a selection of the results is presented.

2 Top-Quark Pair Production

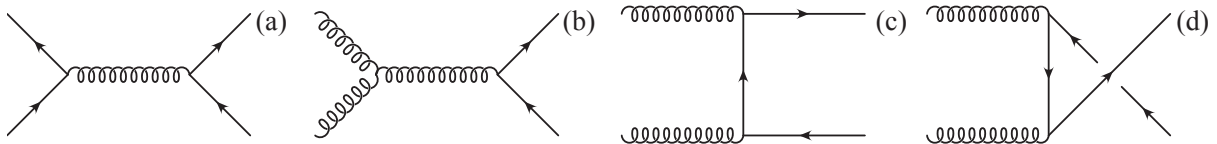


Fig. 1. Leading-order Feynman diagrams contributing to top-quark pair production in hadronic collisions.

In hadronic collisions, top-quark pairs are dominantly produced through the strong interaction. At the parton level, the production mechanisms are quark-antiquark annihilation and gluon fusion. Figure 1 shows the corresponding leading-order (LO) Feynman diagrams. The differential cross section for quark-antiquark annihilation can easily be obtained from $e^+e^- \rightarrow \mu^+\mu^-$ by replacing the QED coupling α_{QED} with the QCD coupling α_s and introducing an appropriate colour factor (2/9) (see also Chap. 5 of Ref. [1]):

$$\frac{d\hat{\sigma}_{q\bar{q} \rightarrow t\bar{t}}}{dz} = \frac{\pi\alpha_s^2}{9s} \beta (2 - (1 - z^2)\beta).$$

Here s denotes the center-of-mass energy squared, $\beta = \sqrt{1 - 4m_t^2/s}$ is the velocity of the top quark in the partonic centre-of-mass system, m_t is the top-quark mass, and $z = \cos(\theta)$ is the cosine of the scattering angle defined as the angle between the incoming quark and the outgoing top quark. The corresponding result for gluon fusion reads

$$\frac{d\hat{\sigma}_{gg \rightarrow t\bar{t}}}{dz} = \frac{\pi\alpha_s^2}{96s} \beta \frac{7 + 9z^2\beta^2}{(1 - z^2\beta^2)^2} (1 + 2\beta^2 - 2z^2\beta^2 - 2\beta^4 + 2z^2\beta^4 - z^4\beta^4).$$

The hadronic cross section is obtained from the partonic cross section through a convolution with the parton distribution functions (PDFs) $f_{i/H}(x, \mu_F)$ which, roughly speaking, describe the probability to find a parton i inside a hadron H with a momentum fraction between x and $x + dx$ of the mother hadron. The factorisation scale μ_F denotes the scale at which, in higher-order calculations, the initial-state singularities are factorised into the parton distribution functions. The final formula for the hadronic cross section is thus given by

$$\begin{aligned} d\sigma_{H_1 H_2 \rightarrow t\bar{t} + X} &= \sum_{i,j} \int dx_1 dx_2 f_{i/H_1}(x_1, \mu_F) f_{j/H_2}(x_2, \mu_F) \\ &\times d\hat{\sigma}_{ij \rightarrow t\bar{t} + X}(x_1 P_1, x_2 P_2, k_t, \alpha_s(\mu_R), \mu_F), \end{aligned} \quad (1)$$

where P_1, P_2 are the momenta of the incoming hadrons, while $k_t, k_{\bar{t}}$ are the momenta of the outgoing top quarks. The sum is over all possible partons. The coupling constant α_s is evaluated at the renormalisation scale μ_R . Note that in higher order, the partonic cross section $d\hat{\sigma}$ also depends on the factorisation scale μ_F such that the factorisation scale dependence of the parton distribution functions is cancelled order by order and the hadronic cross section becomes independent of the non-physical scale μ_F at fixed order in perturbation theory. For more details we refer to Chap. 5 of Ref. [1]. Because the QCD coupling constant is not small ($\alpha_s \approx 0.1$), higher-order corrections can give sizeable contributions and need to be taken into account in most cases. Since the top-quark mass sets a large energy scale, non-perturbative effects are essentially cut off and QCD perturbation theory is believed to give reliable predictions. The next-to-leading order (NLO) QCD corrections for $t\bar{t}$ production were calculated a long time ago [7, 8]. Further improvements were obtained by resumming soft-gluon corrections, which lead to a logarithmic enhancement of the cross section, to next-to-leading logarithmic accuracy [9–11]. Soft-gluon resummation has been extended recently to the next-to-next-to-leading logarithmic (NNLL) accuracy [12–16]. Despite the fact that top quarks do not form bound states (because of their short lifetime), binding effects still lead to minor corrections of the cross section close to the $t\bar{t}$ -pair production threshold. In principle, such a would-be bound state could be observed as a narrow peak in the $t\bar{t}$ invariant-mass spectrum, just below the production threshold. However, the energy resolution of the LHC experiments is not sufficient to resolve this effect.¹ The corresponding corrections to the inclusive cross section are small and have been studied in detail [16–18]. Electroweak corrections have also been investigated [19–25]. For the inclusive cross section of $t\bar{t}$ production at the LHC operating at 14 TeV, they are negative and at the percent level. On the other hand, weak Sudakov logarithms can result in suppression of the cross section at the level of 10–20% for differential distributions at large momentum transfer (see also Chap. 4 of Ref. [1]). Since this region is precisely the one where new heavy resonances could lead to an increase of the cross section, neglecting weak corrections could potentially hide signs of new physics.

Very recently, full next-to-next-to-leading order (NNLO) QCD corrections have been presented for the inclusive cross section [26]. For a centre-of-mass energy of 8 TeV, the result—including soft-gluon resummation at NNLL accuracy (assuming $m_t = 173.3$ GeV and the MSTW2008nnlo68cl PDF set [27])—reads

$$\sigma_{t\bar{t}}(\sqrt{s} = 8 \text{ TeV}) = 245.8^{+6.2}_{-8.4} (\text{scale})^{+6.2}_{-6.4} (\text{PDF}) \text{ pb}. \quad (2)$$

Note that the result does not include the aforementioned weak corrections. The first uncertainty is due to the residual² scale dependence which is used as an estimate of the unknown higher-order contributions. It has been determined by a variation of the renormalisation and factorisation scales in the range $m_t/2 \dots 2m_t$. The second uncertainty is due to the incomplete knowledge of the parton distribution functions. From equation (2) we conclude that the total cross section is known with a precision better than 5%. Moving to higher collider energies will slightly improve the PDF uncertainties since less weight is put to the large x region where the PDFs are less precisely known.

So far, only very few NNLO results exist for differential distributions. Most predictions are currently restricted to NLO accuracy (extended in some cases by the resummation of soft-gluon corrections). Fixed-order NLO corrections are available, for example, through the parton-level Monte Carlo (MC) program MCFM [28]. Combining parton-level NLO calculations with parton-shower simulations is in general not straight forward. A naive combination would count real emission processes twice, since real emission is simulated through the parton shower, but, on the other hand, is also explicitly taken into account in the real-emission processes contributing at NLO. A consistent matching that avoids double-counting has been developed in the past [29, 30]. Differential distributions for top-quark pair production at NLO including parton shower effects are given in [31, 32].

In all calculations mentioned before, the production of stable top quarks is assumed, which is then followed by an on-shell decay. This corresponds to the “narrow-width” or “double-pole approximation”. The naive expectation is that corrections to this approximation should be suppressed like Γ_t/m_t or even Γ_t^2/m_t^2 , where Γ_t denotes the top-quark decay width (see also Ref. [33]). Obviously, the naive expectation can only be true if the observable under consideration is not directly related to off-shell effects. A counter-example is the invariant-mass distribution of the top-quark decay products. Off-shell effects for $t\bar{t}$ production have been investigated in detail in Refs. [34–36], where the QCD NLO corrections for the process $pp \rightarrow W^+W^-b\bar{b}$ have been calculated. Indeed, the effects are typically small, unless observables of the type mentioned before are studied.

As can be seen from the vast amount of different theoretical studies, $t\bar{t}$ production is well understood in the Standard Model. A variety of different corrections have been considered in the past, and precise

¹At a future e^+e^- collider, operating at the top-quark production threshold, the effect would be visible thanks to the high energy resolution and could be used for very precise measurements of the top-quark mass.

²We call the remaining scale dependence “residual” because it is formally of higher order.

theoretical predictions for inclusive as well as differential quantities are available. Top-quark pair production is thus an ideal laboratory to test the consistency of the SM and to search for possible deviations. In the following sections we describe the measurements of inclusive and exclusive cross sections for top-quark pair production.

2.1 Inclusive $t\bar{t}$ Cross Section

First measurements of the inclusive $t\bar{t}$ cross section were published by the ATLAS and CMS collaborations already in the year 2010 [37, 38]. These are based on data corresponding to an integrated luminosity of about 3 pb^{-1} , a fraction of the data collected in 2010. More precise measurements, based on the full 2010 data sample corresponding to an integrated luminosity of 35 pb^{-1} became available shortly after [39–43].

The amount of data collected in the years 2011 ($\sqrt{s} = 7 \text{ TeV}$) and 2012 ($\sqrt{s} = 8 \text{ TeV}$) correspond to integrated luminosities of about 5 and 20 fb^{-1} , respectively—altogether more than a factor 500 more than that of 2010. With this wealth of data, top-quark physics entered a completely new realm of precision and detail. With the 2011 data samples, measurements of the inclusive top-quark pair cross section were performed in all decay channels of the $t\bar{t}$ system (except the one with two τ leptons in the final state), reaching an unprecedented level of statistical and systematic precision [44–54].

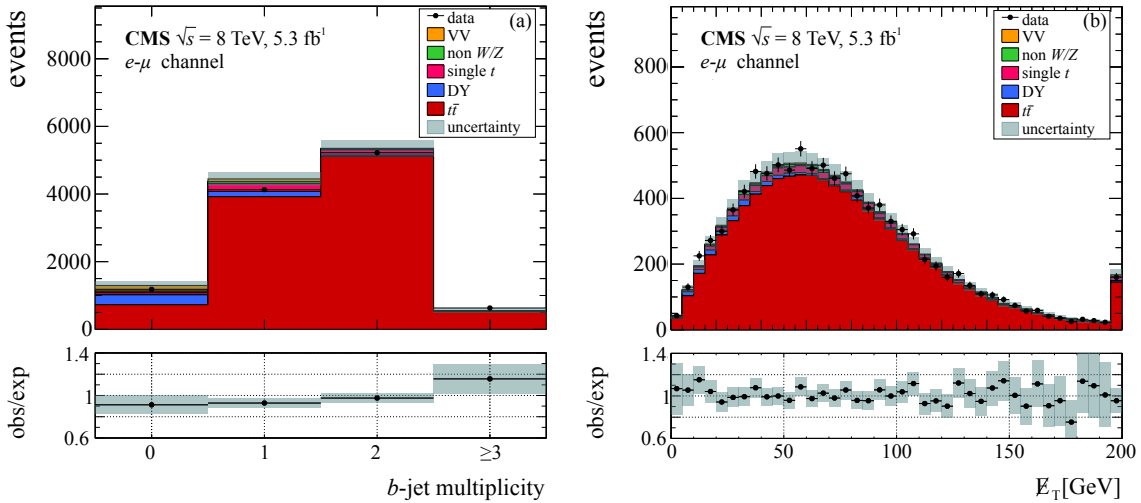


Fig. 2. Distributions of the b -tag multiplicity and missing transverse momentum of the CMS event sample used for the measurement of the inclusive $t\bar{t}$ cross section at a centre-of-mass energy of 8 TeV. (Adapted from Ref. [55].)

In the limit of large statistics, the most precise measurements of the inclusive $t\bar{t}$ cross section can be obtained in the $e\mu$ channel, as the backgrounds and associated uncertainties are minimal. The first published measurement of the top-pair cross section at a centre-of-mass energy of 8 TeV was performed by CMS [55]. It makes use of the decay channel of top-quark pairs with two opposite-charge leptons, one electron and one muon, in the final state. In this channel, backgrounds from non-top-quark events are minimal. Dominant contributions arise from Drell-Yan processes with two τ leptons in the final state that both decay into a lepton. These backgrounds are suppressed by requiring at least one of the two jets to be b -tagged. Smaller background contributions come from single top-quark production (see section 6) and from top-quark events in other decay channels where one of the jets is misidentified as a lepton. In figure 2 the distributions of the b -tag multiplicity and the missing transverse momentum after the final event selection are shown. The final result of this measurement is $\sigma_{t\bar{t}}(\sqrt{s} = 8 \text{ TeV}) = 239.0 \pm 2.1 \text{ (stat)} \pm 11.3 \text{ (syst)} \pm 6.2 \text{ (lumi)} \text{ pb}$, in good agreement with the NNLO prediction quoted in equation (2).

Most recently, the ATLAS collaboration published a measurement yielding the most precise experimental result [54]. In this analysis the numbers of events with exactly one and with exactly two b -tagged jets are counted and used to simultaneously determine $\sigma_{t\bar{t}}$ and the efficiency to reconstruct and b -tag a jet from a top-quark decay, thereby minimising the associated systematic uncertainties.

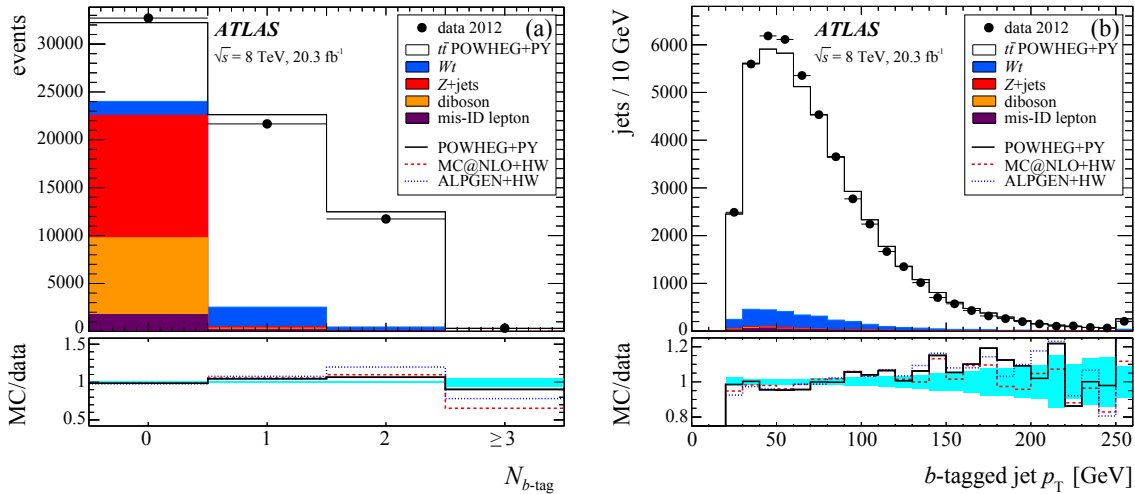


Fig. 3. Distributions of the b -tag multiplicity and b -jet transverse momentum of the ATLAS event sample used for the measurement of the inclusive $t\bar{t}$ cross section at a centre-of-mass energy of 8 TeV. (*Adapted from Ref. [54].*)

In figure 3 the distributions of the b -tag multiplicity and the transverse momentum of the b -tagged jets are displayed. The cross sections for centre-of-mass energies $\sqrt{s} = 7$ TeV and 8 TeV are measured to be $\sigma_{t\bar{t}}(\sqrt{s} = 7 \text{ TeV}) = 182.9 \pm 3.1 \text{ (stat)} \pm 4.2 \text{ (syst)} \pm 3.6 \text{ (lumi)} \pm 3.3 \text{ (beam) pb}$, and $\sigma_{t\bar{t}}(\sqrt{s} = 8 \text{ TeV}) = 242.4 \pm 1.7 \text{ (stat)} \pm 5.5 \text{ (syst)} \pm 7.5 \text{ (lumi)} \pm 4.2 \text{ (beam) pb}$, respectively, where the latter uncertainty is due to the beam-energy uncertainty.

2.2 Differential $t\bar{t}$ Cross Sections

Additional information about top-quark production and decay can be gained from measurements of differential distributions. These do not only probe QCD predictions and provide input to an improved choice of QCD model and scale parameters, but they also have the potential to constrain the parton distribution functions of gluons at large momentum fractions x . Moreover, the differential distributions are potentially sensitive to new physics, e.g. to decays of massive Z -like bosons into top-quark pairs that would become visible at high $t\bar{t}$ invariant masses (see also Chap. 11 of Ref. [1]).

The kinematic properties of a top-quark pair are determined from the four-momenta of all final-state objects by means of reconstruction algorithms. For a general introduction to the different decay channels, see e.g. Ref. [56] and references therein. In the single-lepton channels, kinematic-fitting algorithms are applied to obtain the kinematics of both top quarks. In the dilepton channels, due to the presence of two neutrinos, the kinematic reconstruction is under-constrained. Ambiguities between several solutions are resolved by prioritisation, e.g. by the use of the expected neutrino energy distribution.

A large number of distributions of the top quark and the top-quark pair system, as well as their decay products, has been measured at the LHC [57–59]. In contrast to the situation at the Tevatron, the large $t\bar{t}$ production rate at the LHC leads to a substantial reduction of the statistical uncertainties in each bin. The ATLAS and CMS collaborations report normalised differential cross sections, i.e. shape measurements, in which normalisation uncertainties are removed. In figure 4 the distributions of the invariant mass and of the transverse momentum of the top-quark pair system as measured by ATLAS are displayed [57]. The data are very well described by the various calculations up to an energy scale of about 1 TeV. The results from CMS agree with these findings [58]. The transverse momentum and rapidity distribution of each of the top quarks were also measured and the results from CMS are presented in figure 5. Different theoretical predictions are confronted with the data, and they are generally found to give a good description of the data. However, most Monte Carlo simulations predict the transverse momentum distribution of the top quarks to be somewhat harder than what is seen in the data. This discrepancy between data and simulation is presently under investigation. For the time being it constitutes an important source of uncertainty for many analyses.

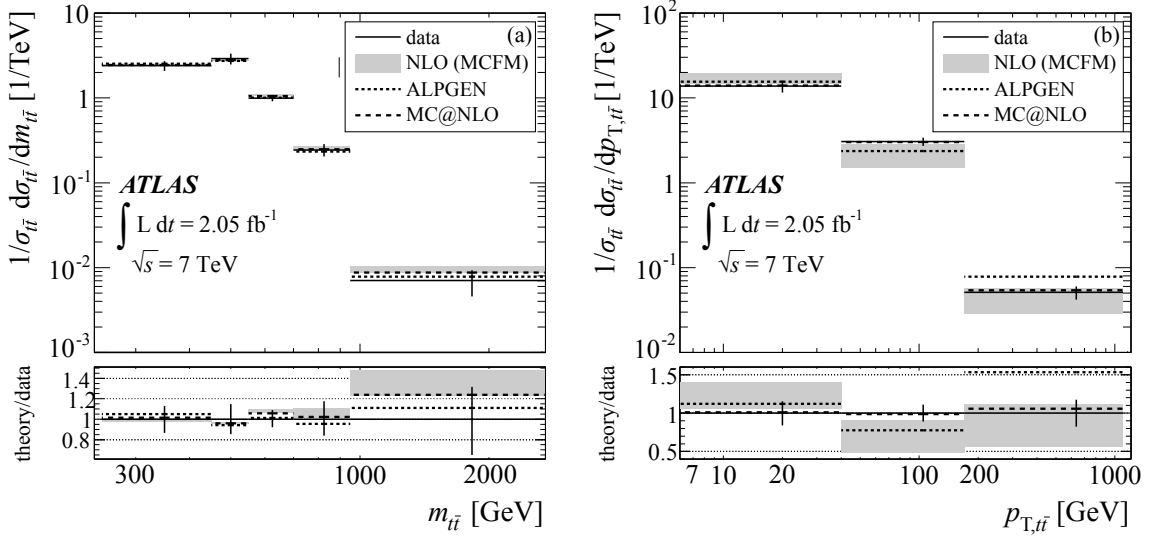


Fig. 4. Normalised differential $t\bar{t}$ production cross sections, measured in pp collisions at a centre-of-mass energy of 7 TeV by the ATLAS collaboration, as a function of (a) the invariant mass of the top-quark pair and (b) the transverse momentum of the top-quark pair system. (*Adapted from Ref. [57].*)

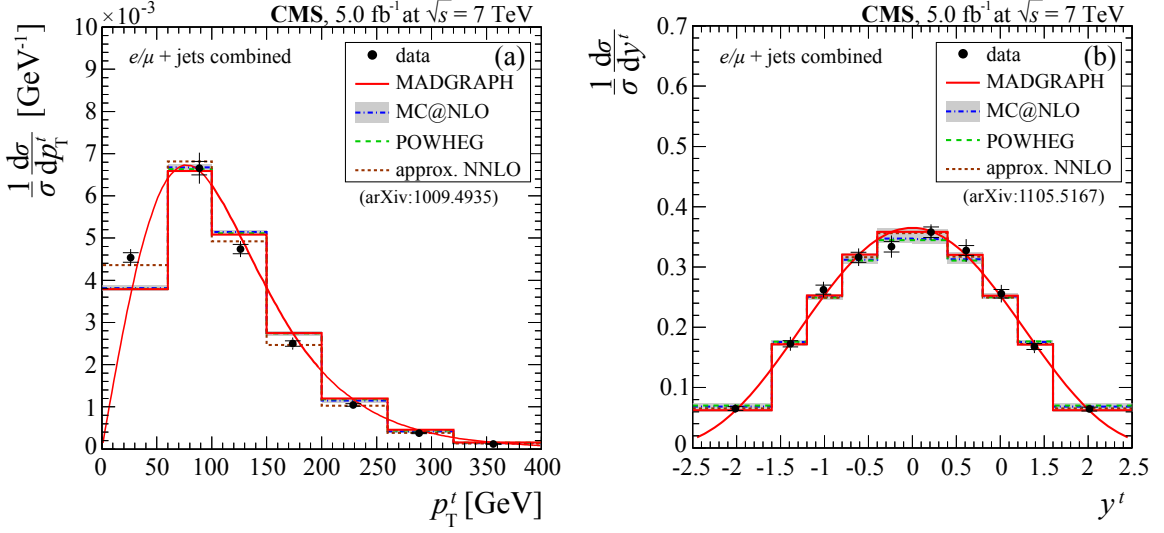


Fig. 5. Normalised differential $t\bar{t}$ production cross sections, measured in pp collisions at a centre-of-mass energy of 7 TeV by the CMS collaboration, as a function of (a) the transverse momentum and (b) the rapidity of each of the top quarks. (*Adapted from Ref. [58].*)

2.3 Top-Quark Pairs and Additional Jets

At LHC energies, a large fraction of top-quark pairs is accompanied by additional high- p_T jets. Demanding, for example, a minimal transverse momentum of 50 GeV for such additional jets, about 30% of all top-quark pairs are produced together with at least one further jet [60]. From an experimental point of view, the jet activity needs to be understood since the appearance of additional jets affects the event reconstruction. Owing to the large rate, $t\bar{t}$ production with jets may also lead to sizeable backgrounds for other SM studies or searches for new physics. As an example, $t\bar{t} + 1\text{-jet} + X$ production is the dominant background for Higgs production via vector-boson fusion. From a theoretical perspective, the additional jet activity can be used for further tests of the underlying production and decay mechanisms. Anomalous $t\bar{t}g$ couplings can be constrained, for example, through a detailed analysis of the process $pp \rightarrow t\bar{t} + 1\text{-jet} + X$. Assuming the validity of our theoretical understanding, $t\bar{t}$ production in association with a jet can also be used to measure the top-quark mass [61]. Since the process $pp \rightarrow t\bar{t} + 1\text{-jet} + X$

is proportional to α_s^3 , NLO contributions can easily give corrections of the order of 30%. For a precise understanding it is thus mandatory to take these corrections into account. In Born approximation, the partonic processes $gg \rightarrow t\bar{t}g$, $q\bar{q} \rightarrow t\bar{t}g$, $qg \rightarrow t\bar{t}q$ and $g\bar{q} \rightarrow t\bar{t}\bar{q}$ contribute to $t\bar{t}$ production in association with a jet. The last three processes are related by crossing. The leading-order partonic matrix elements can be calculated e.g. with the help of MADGRAPH [62]. The hadronic cross sections are then calculable through a numerical Monte Carlo integration, using again equation (1). For the evaluation of the NLO corrections, the one-loop corrections to the aforementioned Born processes, together with real-emission processes, need to be evaluated. Since the two contributions are individually infrared (IR) divergent—the divergences cancel only in the sum—a method to organise this cancellation needs to be applied. In Refs. [60, 63], the one-loop amplitudes have been calculated using a traditional tensor reduction for the one-loop integrals. The cancellation of the IR divergences is achieved using the Catani–Seymour subtraction method [64, 65]. In Ref. [66], an alternative calculation of the NLO corrections, based on the unitarity method, has been presented. In a subsequent study [67], also the on-shell decay of the top quark has been taken into account. NLO results for $t\bar{t}$ production in association with a photon are also available at NLO QCD [68], since this process is closely related to $t\bar{t}$ production in association with jets. In figure 6(a), the cross section for $t\bar{t} + 1\text{-jet} + X$ production is shown as a function of the renormalisation scale μ_R which is set equal to the factorisation scale. For the parton distribution functions the CTEQ6 set [69] has been used.

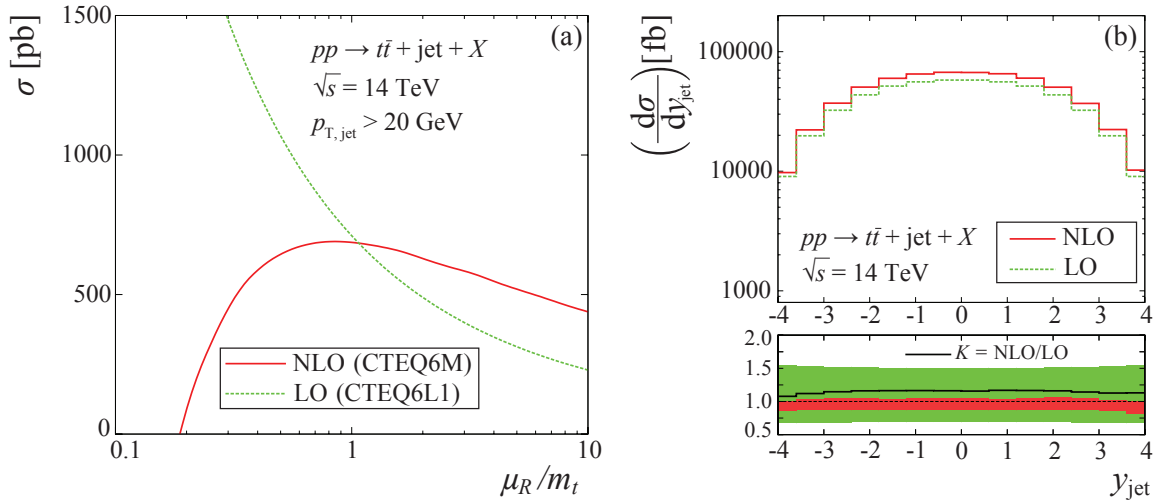


Fig. 6. (a) Cross section for $t\bar{t} + 1\text{-jet} + X$ production at $\sqrt{s} = 14 \text{ TeV}$ as a function of the renormalisation scale. (b) Rapidity distribution of the additional jet at NLO. (*Adapted from Refs. [60, 63].*)

The transverse momentum of the additional jet is required to be at least 20 GeV. The leading-order result strongly depends on the renormalisation scale μ_R , a fact that directly reflects the running of the coupling constant $\alpha_s(\mu_R)$. The Born approximation can thus at best be considered as a rough estimate of the cross section. The NLO corrections as a function of the renormalisation scale, however, show a flat behaviour around $\mu_R = m_t$. This may be considered as an indication that m_t provides a natural scale for this process. It can also be seen from figure 6(a) that the corrections are rather small for $\mu_R = m_t$. Similar observations can be made in figure 6(b) where the rapidity distribution of the additional jet, calculated at NLO, is shown. In Refs. [60, 68] a large variety of differential distributions have been investigated. In particular the transverse momentum distribution of the top quark, the $t\bar{t}$ system and the additional jet have been calculated. It turns out that for large transverse momentum p_T , significant QCD corrections together with a large scale uncertainty are observed. In principle, this is not surprising since at a large transverse momentum an additional scale—different from m_t —is introduced. It is conceivable that a phase-space-dependent renormalisation scale could improve the behaviour of the perturbation theory by effectively resumming large logarithmic corrections. In table 1, the dependence of the cross section on the required minimal transverse momentum of the additional jet, p_T^{cut} , is shown. A strong dependence on p_T^{cut} is found. For $p_T^{\text{cut}} \rightarrow 0$ the cross section diverges logarithmically (the divergence cancels a similar divergence in the cross section for inclusive $t\bar{t}$ production at NNLO, when $t\bar{t} + 1\text{-jet} + X$ production is combined with the two-loop corrections to inclusive $t\bar{t}$ production). With the exception of $p_T^{\text{cut}} = 20 \text{ GeV}$,

| p_T^{cut} [GeV] | $\sigma_{pp \rightarrow t\bar{t} + 1\text{-jet} + X}$ [pb] | |
|--------------------------|--|--------------------------|
| | LO | NLO |
| 20 | $710.8(8)^{+358}_{-221}$ | $692(3)^{+40}_{-62}$ |
| 50 | $326.6(4)^{+168}_{-103}$ | $376.2(6)^{+17}_{-48}$ |
| 100 | $146.7(2)^{+77}_{-47}$ | $175.0(2)^{+10}_{-24}$ |
| 200 | $46.67(6)^{+26}_{-15}$ | $52.81(8)^{+0.8}_{-6.7}$ |

Table 1. Cross section $\sigma_{pp \rightarrow t\bar{t} + 1\text{-jet} + X}$ at the LHC for different values of p_T^{cut} for $\mu = \mu_F = \mu_R = m_t$ [60]. The uncertainties correspond to changes in the scale, namely $\mu = m_t/2$ and $\mu = 2m_t$. In parentheses the uncertainties due to Monte Carlo integrations are quoted.

where very small and negative corrections are observed, the corrections are positive and typically about 15–20%.

Recently, NLO corrections for $t\bar{t}$ production in association with two additional jets were studied. For details, we refer to the original work [70–75].

The ATLAS and CMS collaborations studied the distributions of jet multiplicities and additional jets due to QCD radiation in detail [76–78]. The multiplicity distributions of jets for $t\bar{t}$ events in the single-lepton channel as measured by the CMS collaboration is shown in figure 7. The data are generally well described by the Monte Carlo predictions obtained using MADGRAPH, POWHEG and MC@NLO. Towards very large multiplicities, the MC@NLO generator interfaced with parton showers from HERWIG predicts significantly less events than MADGRAPH or POWHEG, which both use PYTHIA to generate the parton showers.

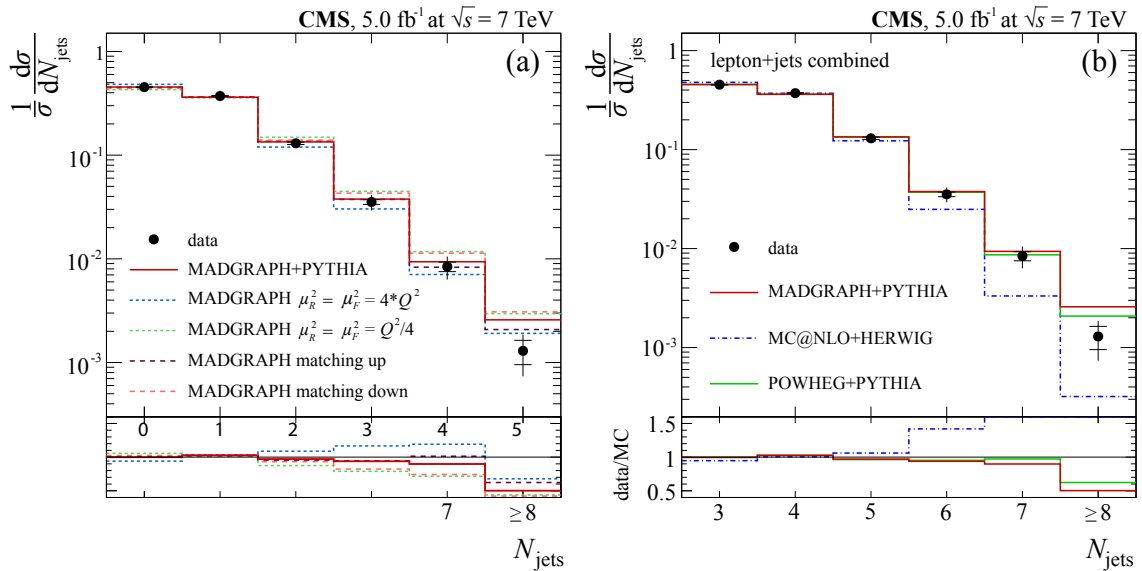


Fig. 7. Differential distributions of jet multiplicity in $t\bar{t}$ events with exactly one lepton and at least three jets in the final state. (a) Data compared with the MADGRAPH simulation for different choices of renormalisation and factorisation scales and the matching scale between matrix element and parton shower. (b) Data compared with several Monte Carlo simulations. (*Adapted from Ref. [76].*)

An alternative way of investigating additional activity in $t\bar{t}$ events is to study “gap-fraction” distributions [76, 77]. In these studies, events are vetoed if they contain an additional jet with transverse momentum above a given threshold in a central rapidity interval. The fraction of events surviving the jet veto, the gap fraction, is presented as a function of the threshold. The gap-fraction distributions for jets as measured by ATLAS are displayed in figure 8. A qualitatively similar trend is observed as in the multiplicity distribution (figure 7) in that the MC@NLO generator predicts a larger fraction of events that have no jet activity beyond the jets originating directly from the top-quark decays. However, vetoing jets just in the forward region, at rapidities $|y| > 1.5$, all simulations predict a smaller fraction of events

with no additional jet than is seen in the data. These results can be used to improve the choice of models, scale parameters and tunes in Monte Carlo simulations for an optimal description of the data.

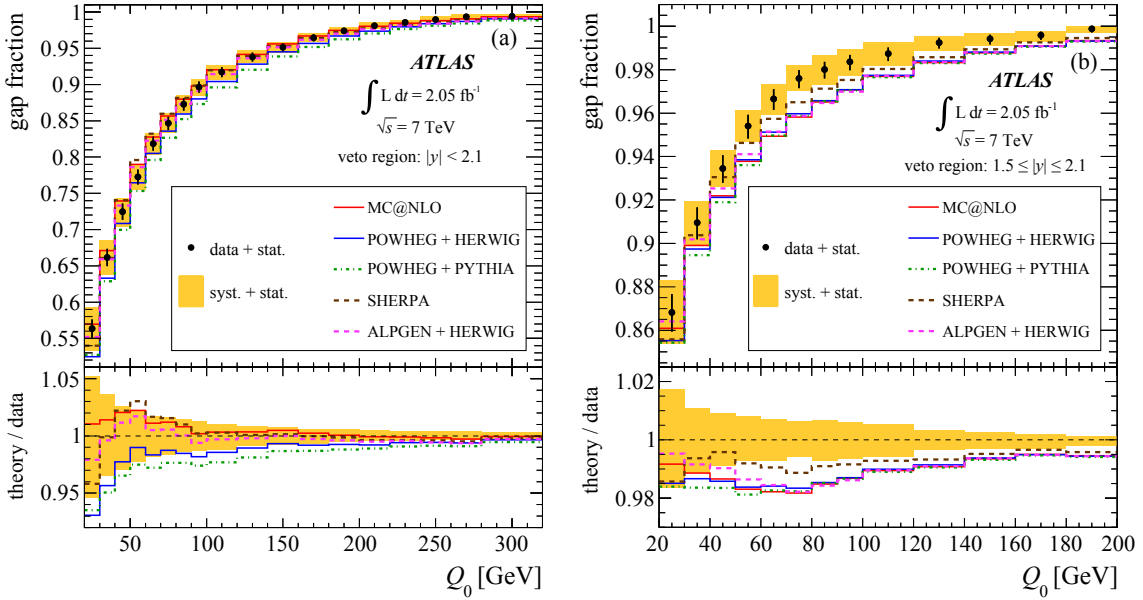


Fig. 8. The measured gap fraction as a function of the jet transverse momentum threshold Q_0 above which there are no additional jets. The data are compared with the predictions from NLO and multi-leg LO MC generators, applying jet vetos in two different rapidity regions (a) $|y| < 2.1$ and (b) $1.5 \leq |y| \leq 2.1$. (Adapted from Ref. [77].)

Building up on the insights about inclusive distributions of additional jets in top-quark pair events, both ATLAS and CMS have also been studying distributions and rates of events with additional jets originating from heavy quarks. These form an important background to events in which Higgs bosons are produced in association with top-quark pairs, with subsequent decay of the Higgs boson into $b\bar{b}$ or $c\bar{c}$ pairs, see Chap. 6 of Ref. [1]. The ATLAS experiment published a measurement of top-quark pairs together with heavy-flavour quarks, $t\bar{t} + b + X$ or $t\bar{t} + c + X$ at $\sqrt{s} = 7$ TeV [79]. The separation between heavy-flavour and light-flavour contents of additional jets is achieved by a fit to the vertex-mass distribution of b -tagged jets, shown in figure 9. From the fit, the relative contribution of heavy quarks is extracted to be $R_{HF} = [6.2 \pm 1.1(\text{stat}) \pm 1.8(\text{syst})]\%$, consistent within uncertainties with leading-order expectations, see Ref. [79] and references therein.

3 Top-Quark Mass

In the SM, the couplings of the top quark to the gauge bosons are governed by the gauge structure (see also Chap. 4 of Ref. [1]). The only free parameters in top-quark physics are thus the three corresponding CKM matrix elements and the top-quark mass, m_t . Instead of the top-quark mass, one may also use the Yukawa coupling λ_t to the Higgs boson as a free parameter since the two are related by $m_t = v/\sqrt{2}\lambda_t$, where v is the vacuum expectation value of the Higgs field. Once the CKM matrix elements and the top-quark mass are known, the SM makes testable predictions for all top-quark properties. Precise measurements of these properties can thus be used to test the consistency of the SM. A prominent example is provided by the simultaneous measurements of the top-quark mass, the W -boson mass and the mass of the Higgs boson since these three masses are related in the SM: The W -boson mass can be calculated as a function of the top-quark mass and the mass of the Higgs boson. A comparison with the measured values thus allows the mechanism of electroweak symmetry breaking predicted by the SM to be indirectly tested. This is demonstrated in figure 10 where, for comparison, also results within the minimal supersymmetric Standard Model (MSSM, see e.g. Chap. 10 of Ref. [1]) are shown [80].

Recently, also the question of vacuum stability has attracted a lot of attention (see for example Refs. [81, 82]). Through quantum corrections, the top quark influences the effective Higgs potential that

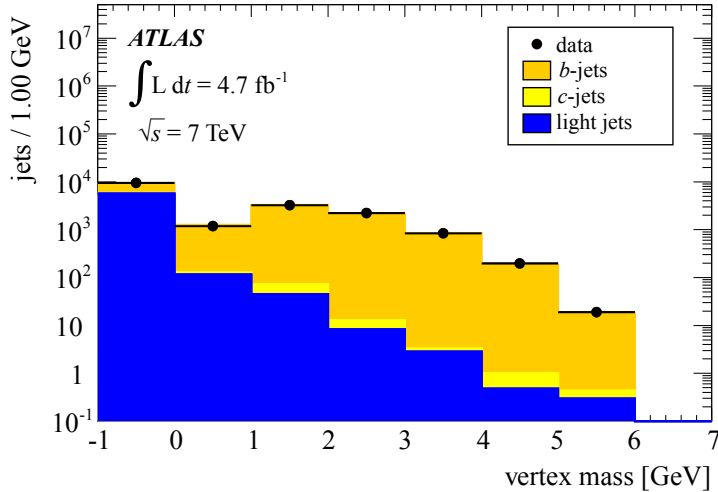


Fig. 9. Vertex-mass distribution for high-purity b -tagged jets in top-quark pair events with two leptons in the final state. For this figure, no cut on the b -tagged jet multiplicity is applied. (*Adapted from Ref. [79].*)

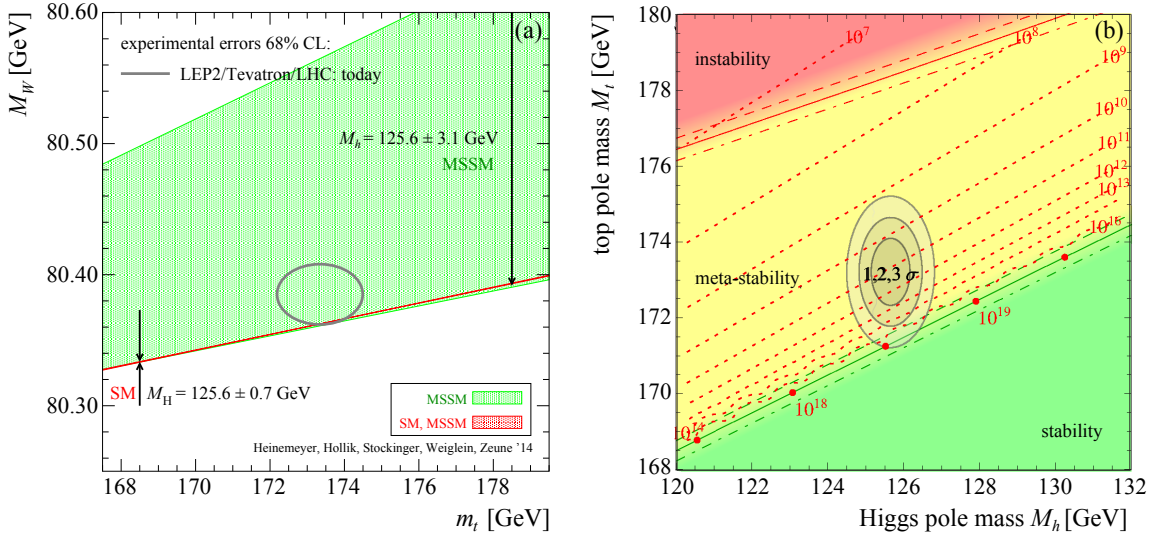


Fig. 10. (a) Consistency of the Standard Model: The W -boson mass as function of the top-quark mass for different Higgs-boson masses. (b) Stability of the vacuum for different top-quark masses. (*Adapted from Refs. [80–82].*)

is responsible for electroweak symmetry breaking. In principle, it is conceivable that these quantum corrections modify the effective potential such that it develops a second minimum or even becomes unbounded from below. As a consequence, the electroweak vacuum might become metastable or even unstable. Calculating the corresponding lifetime of the vacuum and comparing it with the age of the universe provides a further consistency test of the SM.

Experimentally, in most measurements, the mass of the top quark is determined through the reconstruction of the top quark's decay products. The top-quark mass can be estimated by comparing the measured values with the value of the mass parameter used in the simulation. Measurements employing this approach generally achieve the most precise results.

In contrast, from a theoretical point of view, a meaningful definition of the top-quark mass requires to specify the renormalisation scheme used to define the parameter in the theoretical predictions. In this respect the top-quark mass should be treated similar to a coupling constant. In the theoretical description of hadronic collisions, the so-called “on-shell” or “pole mass” scheme and the “minimal subtraction scheme” ($\overline{\text{MS}}$) are commonly used. Quantitatively, the pole mass and the mass measured from final state reconstruction are expected to agree within $\mathcal{O}(1 \text{ GeV})$ [83, 84].

In the pole mass scheme, the renormalised mass is defined as the location of the pole of the renormalised quark propagator, including higher-order corrections. In the (modified) minimal subtraction scheme, the renormalised parameters are defined through a minimal subtraction of the ultraviolet (UV) divergences. The renormalisation constants are chosen such that they just cancel the UV divergences encountered in the loop corrections (together with some irrelevant transcendental constants in the modified minimal subtraction scheme). The two definitions are related in perturbation theory. At NLO accuracy, for example, the relation reads

$$m_t^{\text{pole}} = \overline{m}_t(\mu_R) \left\{ 1 + \frac{\alpha_s(\mu_R)}{\pi} C_F \left[1 - \frac{3}{4} \ln \left(\frac{\overline{m}_t(\mu_R)^2}{\mu_R^2} \right) \right] \right\}, \quad (3)$$

where m_t^{pole} defines the pole mass and $\overline{m}_t(\mu_R)$ defines the mass in the modified minimal subtraction scheme. $C_F = 4/3$ denotes the Casimir operator in the fundamental representation. The $\overline{\text{MS}}$ mass $\overline{m}_t(\mu_R)$ depends on the renormalisation scale, which coins the term “running mass”.

The pole mass scheme is closely related to the intuitive understanding of the mass of a free particle. While for many applications this intuitive picture is a good approximation—for many purposes the top quark behaves like a free quark—it should be clear that this picture is doomed to fail if it comes to ultimate precision. Indeed, it has been shown that the pole mass suffers from the so-called “renormalon ambiguity” that leads to an intrinsic uncertainty of the pole mass of the order of Λ_{QCD} [85, 86]. Despite the fact that the pole mass and the $\overline{\text{MS}}$ mass definitions are related in perturbation theory, it is in practice not straightforward to convert theoretical results from one scheme to the other. So far, this translation has only been calculated for the inclusive cross section for $t\bar{t}$ production and for a few differential distributions in $t\bar{t}$ production.

Experimentally, the top-quark mass has been measured at the LHC using a large variety of methods and observables, and in different decay channels [41, 87–92]. In addition, the difference of the masses of top quarks and antiquarks have been measured [93, 94].

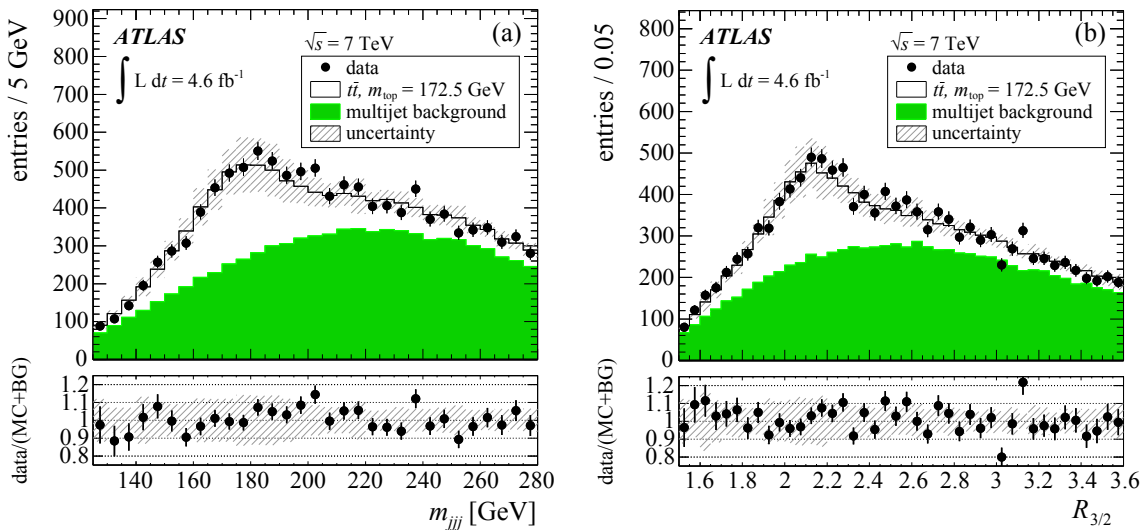


Fig. 11. Distributions of (a) the 3-jet invariant mass and (b) the ratio of the three-jet mass to the dijet mass $R_{3/2}$, measured in data and compared to expectations after applying all event selection criteria. The open histograms show the expected distributions for $t\bar{t}$ events for a top-quark mass value of 172.5 GeV. The shaded histograms indicate the contribution from multi-jet backgrounds. (*Adapted from Ref. [92].*)

A recent measurement using $t\bar{t}$ events with fully hadronic final states is presented by the ATLAS collaboration [92]. Events are selected if they contain at least six jets, and exactly two b -tagged jets are required to be among the four leading jets. The top-quark mass is extracted from a binned likelihood fit to the $R_{3/2}$ distribution, shown in figure 11, where $R_{3/2}$ is the ratio of the reconstructed three-jet and two-jet masses. In this distribution systematic effects that are common to the masses of the reconstructed top quark and the associated W boson cancel. The contribution from multi-jet backgrounds is determined from the data using the event yields in different regions of b -tag jet multiplicity and 6th-jet momentum.

The measurement yields a value for the top-quark mass of

$$m_t = 175.1 \pm 1.4 \text{ (stat)} \pm 1.2 \text{ (syst)} \text{ GeV}.$$

The systematic uncertainties are dominated by the residual uncertainties of the jet energy scale, in particular for b -quark jets, and by the uncertainties from hadronisation modelling.

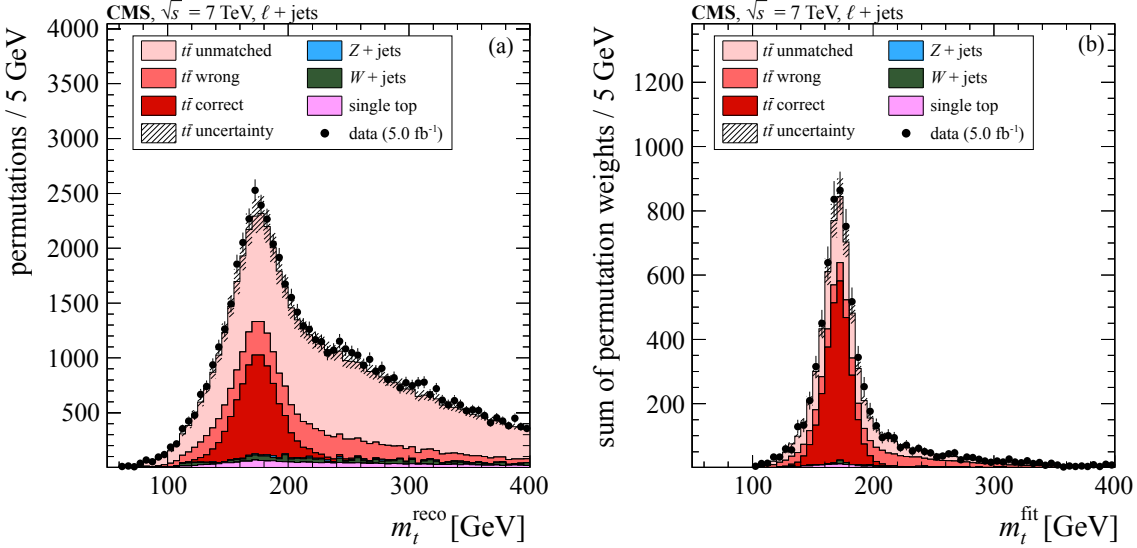


Fig. 12. Reconstructed top-quark mass distributions (a) before and (b) fitted top-quark mass distributions after kinematic reconstruction with entries weighted by the reconstructed goodness-of-fit parameter P_{gof} . (Adapted from Ref. [91].)

The CMS collaboration presented a measurement of the top-quark mass using the full data set collected at a centre-of-mass energy of $\sqrt{s} = 7$ TeV with one electron or muon and at least four jets in the final state [91]. A kinematic fit to the four leading jets, the lepton and the missing transverse momentum is employed to constrain the selected events to the hypothesis of the production of two heavy particles of equal mass, each one decaying to a W boson and a b quark. The reconstructed masses of the two W bosons are constrained in the fit to 80.4 GeV. The reconstructed invariant-mass distribution is shown in figure 12. Events can enter the distributions with different parton-jet assignments (permutations). For simulated $t\bar{t}$ events, the parton-jet assignments can be classified as correct, wrong and unmatched permutations where, in the latter, at least one quark from the $t\bar{t}$ decay is not matched to any of the four selected jets. The actual top-quark mass value is determined simultaneously with the jet energy scale using a joint likelihood fit. The joint likelihood is constructed based on the “ideogram method” in which the likelihood for each event is evaluated from analytic expressions obtained from simulated events. Biases arising due to this method are determined using pseudo-experiments and corrections are applied accordingly. The dominant uncertainty of the final result comes from the uncertainty of the difference in the jet energy responses for jets originating from light (u, d, s) or bottom quarks, as well as from statistical uncertainties in the determination of differences between different models for colour-reconnection processes. The final result is

$$m_t = 173.49 \pm 0.43 \text{ (stat+JES)} \pm 0.98 \text{ (syst)} \text{ GeV},$$

corresponding to an optimal jet energy scale correction of 0.994 ± 0.003 (stat) ± 0.008 (syst) with respect to the CMS calibration.

In spring 2014, this and other precise results from the LHC and the Tevatron, both preliminary and final, were combined to obtain a first world average of the top-quark mass [95]. A summary is shown in figure 13.

An alternative approach to the determination of the top-quark mass is to extract its value from the measured inclusive cross section. This approach has the advantage that the cross section and the pole mass are directly related, such that the extraction yields a theoretically well-defined quantity. Both ATLAS and

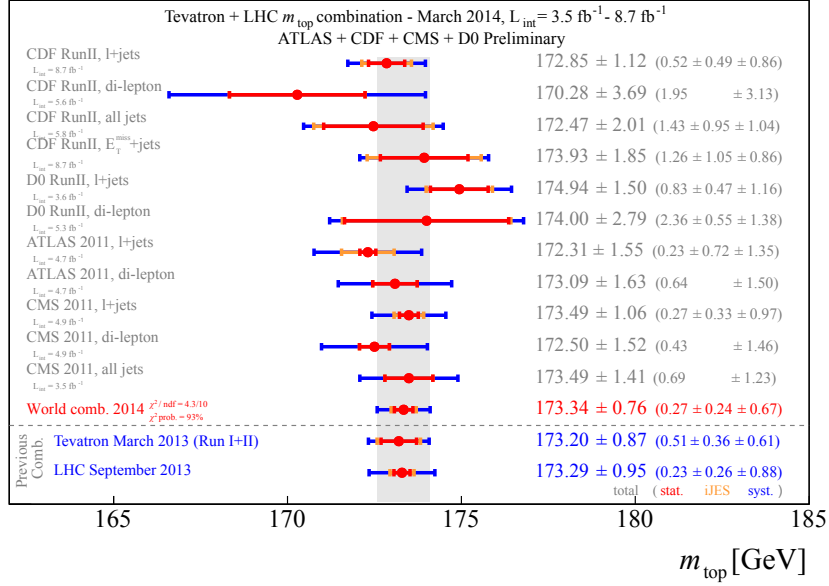


Fig. 13. Mass measurements included in the world combination 2014. Also shown are the results from the combinations of LHC-only data and Tevatron-only data. (Adapted from Ref. [95].)

CMS have used their cross-section measurements to extract the top-quark pole mass [54, 96] as defined at NNLO accuracy [26]. The extractions are performed for different parton distribution functions and take into account the experimental dependence of the measured cross section on the assumed top-quark mass. A summary of the results is shown in figure 14. Conversely, assuming equality between the pole mass and

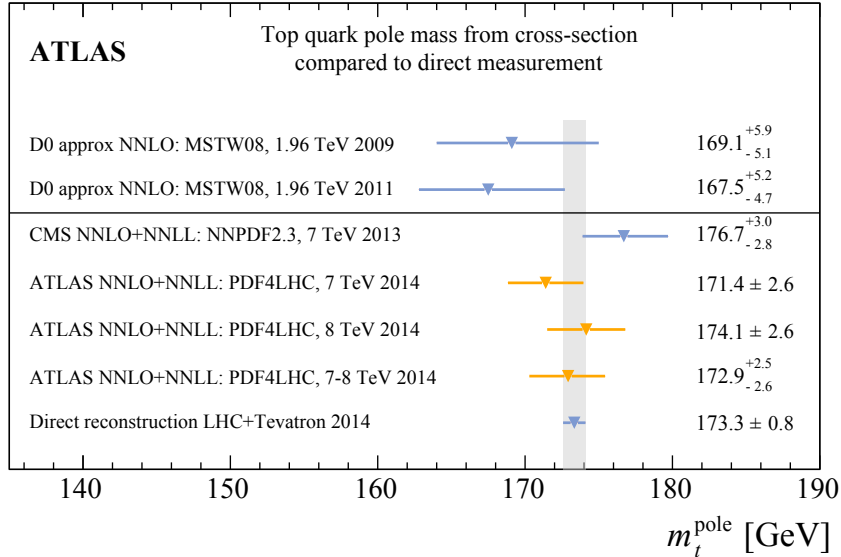


Fig. 14. Summary of determinations of the top-quark pole mass from cross-section measurements. Also shown is the top-quark mass world average as obtained from combination of direct experimental measurements [95]. (Adapted from Ref. [54].)

the directly measured mass within 1 GeV, the cross-section measurements can be used to determine the strong coupling constant α_s [96].

4 Tests of QCD Predictions

Perturbative QCD (pQCD) is a fundamental building block for the understanding of physics processes at the LHC. In addition to cross-section predictions, several other aspects of pQCD can be probed in the top-quark sector. Examples are the small but finite charge asymmetry of $t\bar{t}$ pairs and the correlation between the top-quark and antiquark spins in $t\bar{t}$ production; both quantities are sensitive to the relative proportions of the different production processes of $t\bar{t}$ pairs. Another example is the polarisation of top quarks in $t\bar{t}$ events, which tests the C and CP structure of $t\bar{t}$ production.

4.1 Charge Asymmetry

At leading order QCD, the reactions $pp \rightarrow t\bar{t}$ and $p\bar{p} \rightarrow t\bar{t}$ are symmetric under the exchange of top quarks and antiquarks. The relevant hard scattering processes are quark-antiquark annihilation, $q\bar{q} \rightarrow t\bar{t}$, and gluon-fusion, $gg \rightarrow t\bar{t}$. At NLO, two additional types of processes have to be considered which break this charge symmetry, namely quark-gluon scattering, $qg \rightarrow t\bar{t}q$, and radiative corrections to quark-antiquark annihilation [97, 98]. In both cases, the charge asymmetry is induced by interference effects, e.g. interference between processes with initial-state and final-state radiation or interference between Born and box diagrams. All gluon-fusion processes are symmetric under the exchange of the top quark and antiquark.

The charge asymmetry results in an asymmetry of the $t\bar{t}$ event kinematics: Top quarks (antiquarks) are preferentially emitted in the direction of the incoming quark (antiquark). The observables with which the charge asymmetry can be measured are chosen depending on the colliding particles and the centre-of-mass energy. Quark-antiquark annihilation dominates the production of $t\bar{t}$ pairs at the Tevatron, and so the top quark and antiquark will preferentially be emitted in the direction of the incoming protons and antiprotons, respectively. The most common observable is thus a forward-backward asymmetry,

$$A^{t\bar{t}} = \frac{N(\Delta y > 0) - N(\Delta y < 0)}{N(\Delta y > 0) + N(\Delta y < 0)},$$

where Δy is the difference between the rapidities of the top quark and antiquark, i.e. $\Delta y = y_t - y_{\bar{t}}$, and N is the number of events. The predictions for this observable depend on several kinematic variables. The inclusive forward-backward asymmetry is predicted to be $A^{t\bar{t}} = 0.088 \pm 0.006$ [99], while for invariant $t\bar{t}$ masses larger than 450 GeV the prediction increases to $A^{t\bar{t}}(m_{t\bar{t}} > 450 \text{ GeV}) = 0.129^{+0.008}_{-0.006}$ [99]. The CDF and DØ experiments have measured the forward-backward asymmetry both inclusively and as a function of several kinematic quantities, e.g. $m_{t\bar{t}}$ [100, 101]. They found an excess compared to the NLO QCD predictions with significances of several standard deviations. Over the last few years these measurements gave rise to speculations about contributions to $t\bar{t}$ production due to physics beyond the Standard Model. Although refined theoretical studies and further measurements appear to have resolved the issue, measurements of the charge asymmetry are still in the focus of the LHC top-physics programme.

At the LHC with its symmetric pp initial state, the charge asymmetry can not be measured as a forward-backward asymmetry. Instead, a central-decentral asymmetry is defined. As valence quarks carry a larger average momentum fraction and top (anti)quarks are produced preferentially in the direction of the incoming (anti)quark, the average top-quark rapidity is larger than that of top antiquarks. A useful observable is defined as

$$A_C = \frac{N(\Delta|y| > 0) - N(\Delta|y| < 0)}{N(\Delta|y| > 0) + N(\Delta|y| < 0)},$$

where $\Delta|y|$ is the difference between the absolute values of the top-quark and top-antiquark rapidities, i.e. $\Delta|y| = |y_t| - |\bar{y}_t|$. The NLO QCD prediction including electroweak effects for the inclusive asymmetry is $A_C = 0.0123 \pm 0.0005$ [99]. Predictions are also available for different values of the invariant mass, the rapidity and the transverse momentum of the $t\bar{t}$ pair, and they range between -0.6% and 2.8% (see discussion in Ref. [102]). The asymmetry depends on the first two variables because they are correlated to the fraction of quark-antiquark annihilation in $t\bar{t}$ production. It depends on the latter quantity because the amount of initial-state and final-state radiation changes with increasing transverse momentum.

After an initial measurement using only a subset of the available data recorded at $\sqrt{s} = 7$ TeV [103], the ATLAS collaboration has studied the charge asymmetry based on the full data set, which corresponds to an integrated luminosity of 4.7 fb^{-1} [102]. Events are selected that are consistent with the single-lepton decay mode of $t\bar{t}$ production. For each event, the top-quark pair is reconstructed using a likelihood-based

kinematic fit [104], and the rapidities of the top quark and antiquark are reconstructed. The measured distribution of $\Delta|y|$ includes background events and is distorted by detector and acceptance effects. A Bayesian unfolding technique [105] is applied on the background-subtracted spectrum to remove such effects. The measured inclusive asymmetry is

$$A_C = 0.006 \pm 0.010,$$

where the largest sources of uncertainty are the statistical uncertainty and the uncertainty due to lepton and jet reconstruction. In addition, the asymmetry for invariant $t\bar{t}$ masses greater than 600 GeV is found to be $A_C(m_{t\bar{t}} > 600 \text{ GeV}) = 0.018 \pm 0.022$, which is in good agreement with the predicted value of $0.0175^{+0.0005}_{-0.0004}$. The asymmetry is also measured as a function of the transverse momentum, the absolute value of the rapidity and the invariant mass of the $t\bar{t}$ pair. The latter measurement is repeated for a subset of the events featuring a high longitudinal $t\bar{t}$ velocity, i.e. requiring $\beta_{z,t\bar{t}} > 0.6$. The asymmetries as a function of the invariant $t\bar{t}$ mass are shown in figure 15 without (a) and with (b) the additional velocity requirement. All four differential measurements are in agreement with the SM predictions.

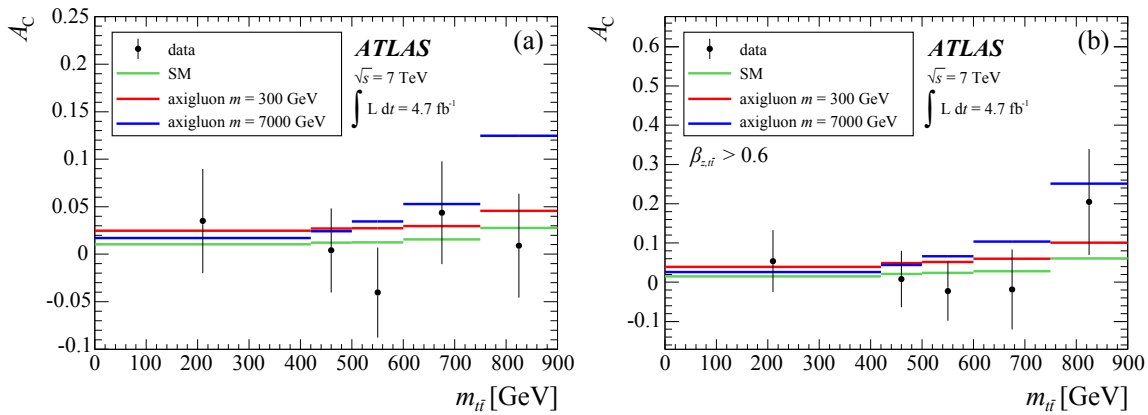


Fig. 15. Charge asymmetry measured by the ATLAS collaboration as a function of the invariant $t\bar{t}$ mass (a) without and (b) with the requirement of a large longitudinal $t\bar{t}$ velocity. (Adapted from Ref. [102].)

The CMS collaboration has measured the charge asymmetry in a data set corresponding to an integrated luminosity of 5.0 fb^{-1} [106, 107] using events with exactly one charged lepton in the final state. After event reconstruction and calculation of the top-quark and top-antiquark rapidities, the $\Delta|y|$ distribution is determined. Subsequently, the estimated background contributions are subtracted from the data and the spectra are corrected for detector and acceptance effects using a regularised unfolding procedure via matrix inversion [108]. The measured inclusive asymmetry is

$$A_C = 0.004 \pm 0.010 \text{ (stat)} \pm 0.011 \text{ (syst)},$$

where the major sources of systematic uncertainty are the residual model dependence of the unfolding procedure and the lepton reconstruction. As in the ATLAS measurement, the asymmetry is also measured as a function of the transverse momentum, the rapidity and the invariant mass of the $t\bar{t}$ system. Figure 16(a) shows the background-subtracted and unfolded $\Delta|y|$ distribution for the inclusive case, and figure 16(b) shows the charge asymmetry as a function of the transverse momentum of the $t\bar{t}$ pair. All measurements are consistent with the SM predictions.

In a further study using the full 7 TeV data set, the CMS collaboration measured the charge asymmetry in a sample of dileptonically decaying $t\bar{t}$ pairs [109]. In addition to the observable A_C , a “lepton charge asymmetry” is defined as

$$A_C^{\text{lep}} = \frac{N(\Delta|\eta_\ell| > 0) - N(\Delta|\eta_\ell| < 0)}{N(\Delta|\eta_\ell| > 0) + N(\Delta|\eta_\ell| < 0)},$$

where $\Delta|\eta_\ell| = |\eta_{\ell+}| - |\eta_{\ell-}|$ and where $\eta_{\ell\pm}$ are the pseudo-rapidities of the positively and negatively charged leptons in each event. The SM prediction for this observable is $A_C^{\text{lep}} = 0.0070 \pm 0.0003$ [99]. The event reconstruction is performed using the “analytical matrix weighting technique” (AMWT) [41]. After

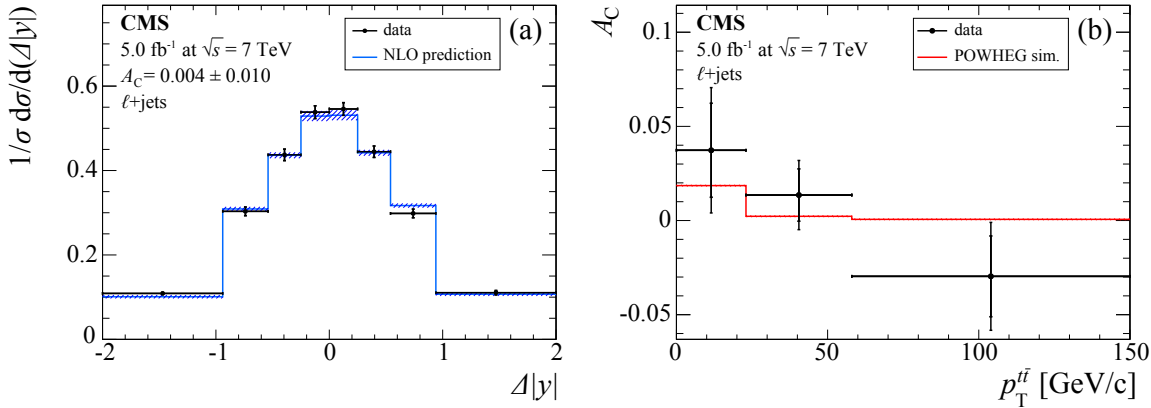


Fig. 16. (a) The background-subtracted and unfolded $\Delta|y|$ distribution obtained by CMS for a single-lepton sample. (b) The charge asymmetry as a function of the transverse momentum of the $t\bar{t}$ pair. (*Adapted from Ref. [107].*)

subtracting all background contributions from the measured $\Delta|y|$ and $\Delta|\eta_\ell|$ distributions, the spectra are unfolded using singular value decomposition [110]. The measured asymmetries are

$$A_C = -0.010 \pm 0.017 \text{ (stat)} \pm 0.008 \text{ (syst) and}$$

$$A_C^{\text{lep}} = 0.009 \pm 0.010 \text{ (stat)} \pm 0.006 \text{ (syst)},$$

where the largest sources of systematic uncertainty are residual biases in the unfolding procedure and uncertainties in the $t\bar{t}$ modelling and the jet reconstruction. The lepton charge asymmetry is also calculated as a function of the same three kinematic variables as for the single-lepton analysis. No deviations between the measurements and the predictions are found.

The charge asymmetry in $t\bar{t}$ production is predicted to cause a small effect on a variety of observables at the LHC. None of the measurements performed by the ATLAS and CMS collaborations are in conflict with the SM predictions while the current experimental precision is of the order of the size of the prediction itself. Although a variety of models of physics beyond the Standard Model can be excluded with the set of measurements already performed, the analysis of the 8 TeV data (which was not finished at the time of publication) will provide further sensitivity to the predictions of perturbative QCD. It should be noted, that the interpretation of the leptonic charge asymmetries relies on a solid understanding of top-quark production and decay. In particular, a non-standard top-quark polarisation could affect the leptonic asymmetries. It is thus important to cross check the polarisation through explicit measurements.

4.2 Top-Quark Polarisation and Spin Correlation in Top-Quark Pairs

Top-quark polarisation in $t\bar{t}$ events and the correlation between the top-quark and antiquark spins in $t\bar{t}$ production are probes of perturbative QCD and observables that are sensitive to anomalous production mechanisms. Measurements of such quantities are only feasible because of the extremely short lifetime of the top quark of $\tau_t \approx 1.5 \cdot 10^{-25}$ s. The lifetime is roughly one order of magnitude smaller than the time scale at which hadronisation takes place, $\tau_{\text{had}} \approx 1/\Lambda_{\text{QCD}} \approx 3 \cdot 10^{-24}$ s, and in particular shorter than the time needed to decorrelate the spin configuration of the $t\bar{t}$ pair, $\tau_{\text{decorr}} \approx \frac{\hbar m_t}{\Lambda_{\text{QCD}}^2} \approx 3 \cdot 10^{-21}$ s [111, 112]. Top quarks will thus decay before they can form bound states. As mentioned before, the large top-quark width cuts off non-perturbative effects. The polarisation of the top-quark is thus not diluted by hadronisation effects and can be calculated reliably within perturbation theory. The parity-violating weak decay can then be used to analyse the top-quark polarisation through the angular distribution of the decay products. The correlation of the top-quark and antiquark spins is reflected in the angular correlation of the top-quark and antiquark decay products. This is a unique feature since all lighter quarks form hadrons for which—due to the hadronisation process—the initial spin information of the mother particle is diluted or even entirely lost. In contrast, the spin information of the top quark is directly transferred to its decay products.

In top-quark pairs, information about the polarisation of top quarks and the correlation between top-quark and antiquark spins can be obtained from the differential cross section

$$\frac{1}{\sigma} \frac{d\sigma}{d \cos(\theta_1) d \cos(\theta_2)} = \frac{1}{4} (1 + \alpha_1 P_1 \cos(\theta_1) + \alpha_2 P_2 \cos(\theta_2) - \alpha_1 \alpha_2 A \cos(\theta_1) \cos(\theta_2)), \quad (4)$$

where $\theta_1(\theta_2)$ are the angles between the momentum direction of a daughter particle of the top (anti)quark and a chosen reference axis. The coefficients $\alpha_1(\alpha_2)$ and $P_1(P_2)$ are the “spin-analysing power” of the daughter particle and the degree of polarisation (with respect to the reference axis) of the top (anti)quark, respectively. The spin-analysing power quantifies the amount of spin information transferred to the daughter particle and depends on the particle type. It is approximately one for charged leptons and down-type quarks from the subsequent decay of the W boson [113]. The coefficient A is a measure of the spin correlation between top quark and antiquark.

As the strong interaction conserves parity, the polarisation of top (anti)quarks in $t\bar{t}$ production within the production plane is expected to be zero. QCD absorptive parts, sometimes also called final-state interactions³, introduce a tiny transverse polarisation at the one-loop level [114, 115]. Electroweak corrections lead to a small amount of net polarisation of $\alpha_i P_i = 0.003 \pm 0.001$ [116]. It can be shown that polarisation can be induced by the imaginary part of a chromo-electric dipole moment which in turn can lead to P -odd and CP -odd terms in the matrix elements [116]. Such effects can stem from processes beyond the SM.

The correlation coefficient A can be expressed as an asymmetry variable in the number of events N with parallel and antiparallel spin,

$$A = \frac{N(\uparrow\uparrow) + N(\downarrow\downarrow) - N(\uparrow\downarrow) - N(\downarrow\uparrow)}{N(\uparrow\uparrow) + N(\downarrow\downarrow) + N(\uparrow\downarrow) + N(\downarrow\uparrow)},$$

where \uparrow and \downarrow indicate the spin projections onto the reference axis. The prediction of the correlation coefficient depends on the particular choice of reference axis. While for measurements at the Tevatron the “off-diagonal basis” and the “beam basis” are suitable choices, measurements at the LHC are most sensitive to the correlation coefficient in the “helicity basis”. In the beam basis, the direction of the beam is used as reference axis for the top-quark as well as for the antiquark. In the helicity basis, the direction of flight of the top-quark/antiquark is used as respective reference axis. The strength of the correlation predicted by the SM using the helicity basis is $A = 0.031$ [117] with an uncertainty of approximately 1%.

Close to the threshold, top-quark pairs produced via gluon fusion are in a 1S_0 state while top-quark pairs produced via quark-antiquark annihilation are in a 3S_1 state. As a consequence, the spins of a top-quark pair produced in quark-antiquark annihilation tend to be parallel while in gluon fusion they tend to be antiparallel. A measurement of the coefficient A is thus a direct probe of the production mechanism. Contributions from additional production mechanisms, e.g. yet unknown intermediate vector bosons, can lead to altered predictions for A . Note that the correlation coefficient depends both on the centre-of-mass energy and on the initial-state particles, and so the measurements conducted at the Tevatron and the LHC are complementary.

While an evidence for correlated spins in top-quark pairs was already reported by the DØ collaboration [118], the hypothesis that the spins of the top quark and the antiquark are uncorrelated was fully disproved for the first time by a measurement of the ATLAS collaboration [119]. The measurement is based on a data set corresponding to an integrated luminosity of 2.1 fb^{-1} recorded at $\sqrt{s} = 7 \text{ TeV}$. Events consistent with the signature of $t\bar{t}$ events decaying in the dilepton mode are selected, and the spin correlation is probed using the difference in azimuthal angle between the two charged leptons, $\Delta\phi$, calculated in the laboratory frame. The advantage of this observable compared to those in equation (4) is that no kinematic reconstruction of the top-quark momenta is necessary while the sensitivity to the correlation strength is largely retained [112]. Figure 17(a) shows the observed $\Delta\phi$ spectrum as well as the predictions for the assumption of SM correlations and the absence of correlations. The measured correlation coefficient is not compatible with zero,

$$A = 0.40 \pm 0.04 \text{ (stat)}^{+0.08}_{-0.07} \text{ (syst)},$$

with a significance of 5.1 standard deviations. The dominating sources of systematic uncertainty are the estimate of events with misidentified leptons and the jet reconstruction. In a second publication based

³These are due to imaginary parts of the loop integrals caused by the on-shell production of intermediate states.

on the full 7 TeV data set [120], the spin correlation is measured in the dilepton channel using a variety of alternative observables, and it is also measured in the single-lepton channel.

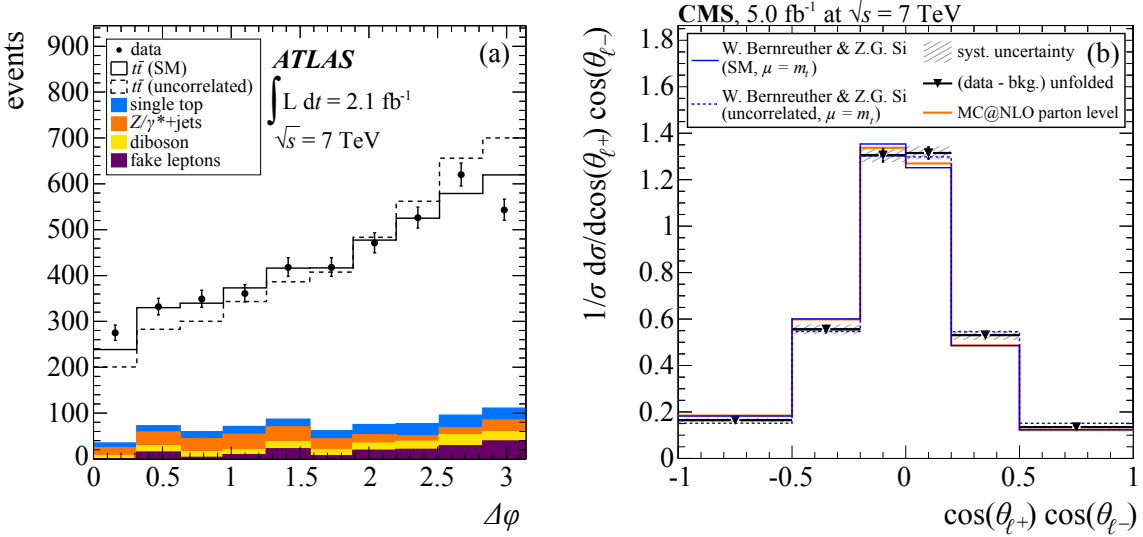


Fig. 17. (a) Observed and predicted $\Delta\phi$ spectrum in a sample of dileptonic $t\bar{t}$ events recorded with the ATLAS experiment. (b) Distribution of $\cos(\theta_{\ell+}) \cos(\theta_{\ell-})$ in dileptonic $t\bar{t}$ events as observed by CMS together with predictions for two different correlation scenarios. (*Adapted from Refs. [119, 121].*)

The CMS collaboration has analysed a data set corresponding to an integrated luminosity of 5.0 fb^{-1} recorded at $\sqrt{s} = 7$ TeV [121]. Events are selected that contain exactly two charged leptons with large transverse momenta. Three angular variables are calculated for each event—the $\Delta\phi$ variable defined earlier as well as the angles $\theta_{\ell+}$ and $\theta_{\ell-}$, which are defined as the angles of the positively and negatively charged lepton in the helicity frame, respectively. From the distributions of these variables, two asymmetries are derived which provide discrimination between the two scenarios of SM correlations and no correlations:

$$A_{\Delta\phi} = \frac{N(\Delta\phi > \pi/2) - N(\Delta\phi < \pi/2)}{N(\Delta\phi > \pi/2) + N(\Delta\phi < \pi/2)},$$

$$A_{\cos\cos} = \frac{N(\cos(\theta_{\ell+}) \cos(\theta_{\ell-}) > 0) - N(\cos(\theta_{\ell+}) \cos(\theta_{\ell-}) < 0)}{N(\cos(\theta_{\ell+}) \cos(\theta_{\ell-}) > 0) + N(\cos(\theta_{\ell+}) \cos(\theta_{\ell-}) < 0)}.$$

The latter asymmetry is a measure for the correlation coefficient in the helicity basis, i.e. $A = -4 \cdot A_{\cos\cos}$ [116]. The predictions at NLO perturbation theory for the case of SM-like correlations (no correlations) are $A_{\Delta\phi} = 0.115^{+0.014}_{-0.016}$ ($A_{\Delta\phi} = 0.210^{+0.013}_{-0.008}$) and $A_{\cos\cos} = -0.078 \pm 0.006$ ($A_{\cos\cos} = 0$), see Refs. [116, 117] and references in Ref. [121]. The angles $\theta_{\ell\pm}$ require the explicit reconstruction of both the top quark and the antiquark, which is done using the AMWT technique. In addition, the relation between the asymmetry variable and the correlation coefficient is valid only if no acceptance cuts and detector effects distort the measurement. The distributions of $\Delta\phi$ and $\cos(\theta_{\ell+}) \cos(\theta_{\ell-})$ are thus unfolded using singular value decomposition. Figure 17(b) shows the unfolded $\cos(\theta_{\ell+}) \cos(\theta_{\ell-})$ distribution and the predictions for the two correlation scenarios. The asymmetries are measured to be

$$A_{\Delta\phi} = 0.133 \pm 0.010 \text{ (stat)} \pm 0.007 \text{ (syst)} \pm 0.012 \text{ (top } p_T \text{) and}$$

$$A_{\cos\cos} = -0.021 \pm 0.023 \text{ (stat)} \pm 0.027 \text{ (syst)} \pm 0.010 \text{ (top } p_T \text{),}$$

where the statistical and systematic uncertainties as well as an uncertainty associated with the modelling of the p_T spectrum of the top quark are given. The largest systematic uncertainties come from the unfolding procedure as well as the jet reconstruction, the background estimate and the modelling of $t\bar{t}$ events.

The measurements conducted by ATLAS and CMS show that the spins of the top quark and the antiquark in $t\bar{t}$ events are indeed correlated and that the amount of correlation is as expected from perturbation theory at NLO. The production mechanisms of $t\bar{t}$ events is thus consistent with that predicted by QCD, and no indications for additional production mechanisms are found.

The polarisation of top quarks in $t\bar{t}$ events is studied by CMS using the same data set and event selection as for the measurement of the $t\bar{t}$ spin correlation [121]. The polarisation is estimated from the unfolded distribution of the angle θ_{ℓ^\pm} and the resulting asymmetry,

$$A_P = \frac{N(\cos(\theta_\ell) > 0) - N(\cos(\theta_\ell) < 0)}{N(\cos(\theta_\ell) > 0) + N(\cos(\theta_\ell) < 0)}.$$

The polarisation in the helicity basis is then $P = 2A_P$. The asymmetry is calculated using positively and negatively charged leptons under the assumption of CP invariance and is measured to be

$$A_P = 0.005 \pm 0.013 \text{ (stat)} \pm 0.020 \text{ (syst)} \pm 0.008 \text{ (top } p_T\text{)},$$

where the uncertainties are again the statistical and systematic ones and the uncertainty due to the mismeasured p_T spectrum of the top quark. The two largest systematic uncertainties are uncertainties on the top-quark mass and on the jet reconstruction.

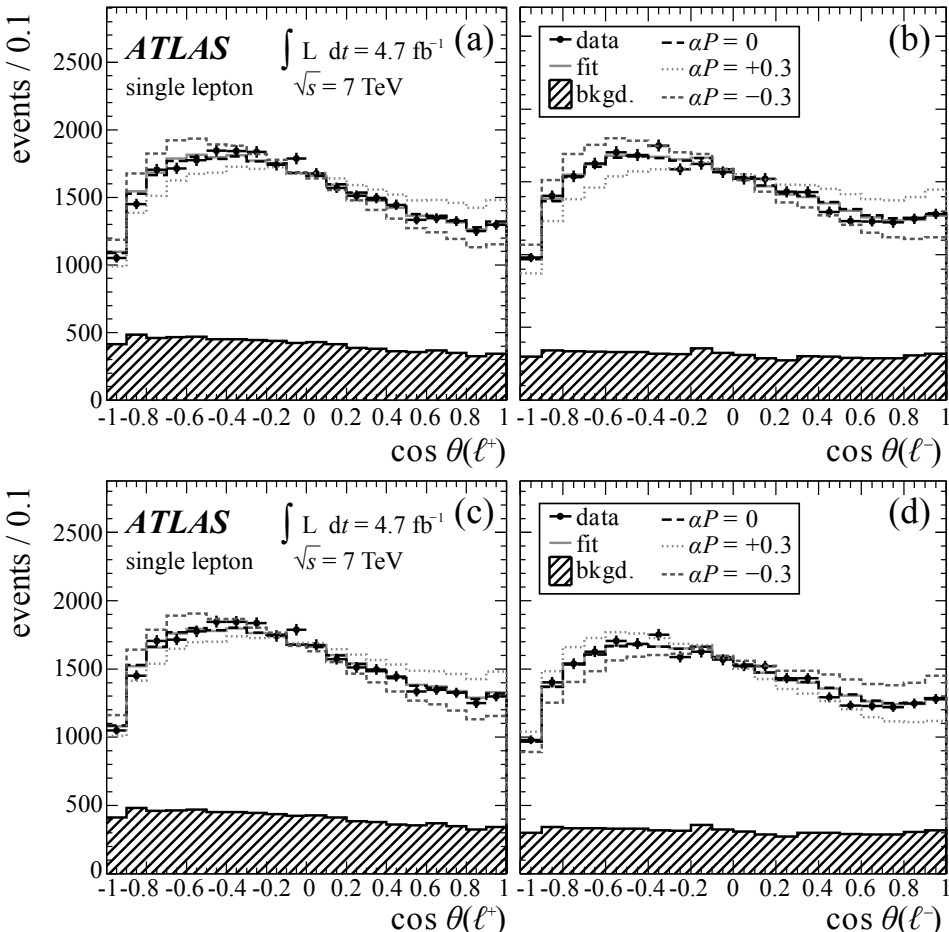


Fig. 18. ATLAS polarisation measurements in the single-lepton channel with three different polarisation assumptions. (a) and (c) show the distributions for positively charged leptons, while (b) and (d) show the distributions for negatively charged leptons. (a),(b) assume CP invariance, while for (c),(d) maximal CP violation is assumed. (Adapted from Ref. [122].)

An ATLAS measurement of the top-quark polarisation [122] uses $t\bar{t}$ events decaying in the single-lepton and dilepton mode. The data were collected at $\sqrt{s} = 7$ TeV and correspond to an integrated luminosity of $4.66 \pm 0.08 \text{ fb}^{-1}$. The full $t\bar{t}$ system is reconstructed using a kinematic likelihood [104] in the single-lepton channel and the neutrino-weighting method [123] in the dilepton channel. The angle θ_{ℓ^\pm} is calculated in the helicity basis for each lepton, and the corresponding distributions are fitted with

templates of partially polarised top quarks. The spin correlation is assumed to be that of the SM. The fits are done separately for each lepton type as well as for positively and negatively charged leptons. The latter is done in order to distinguish scenarios in which the polarisation comes from CP -conserving processes and maximally CP -violating processes. For such cases, the expressions $\alpha_\ell P$ are either the same for top quark and antiquark, or they differ by a sign. Figure 18 shows the distributions of $\cos(\theta_{\ell^\pm})$ measured in single-lepton events for the two scenarios. The combined polarisation measured for the two scenarios is

$$\begin{aligned}\alpha_\ell P &= -0.035 \pm 0.014 \text{ (stat)} \pm 0.037 \text{ (syst)} \text{ (CP invariance)}, \\ \alpha_\ell P &= 0.020 \pm 0.016 \text{ (stat)}^{+0.013}_{-0.017} \text{ (syst)} \text{ (CP violation)}.\end{aligned}$$

The major systematic uncertainty stems from the jet reconstruction.

The ATLAS and CMS measurements are both consistent with the SM prediction that top quarks produced in $t\bar{t}$ pairs via the strong interaction are not polarised.

5 Tests of Electroweak Predictions

Studies of the electroweak couplings of the top quark comprise measurements of a number of different observables. While the polarisation of W bosons from top-quark decays is a consequence of the $V-A$ structure of the Wtb vertex, the cross sections for single top-quark production depend directly on the strength of the coupling to W bosons (see section 6). The coupling strength to Z bosons and photons can be probed by measurements of $t\bar{t}$ production with additional such bosons.

5.1 W -Boson Polarisation

The massive W bosons produced in top-quark decays are real spin-1 particles and thus have three possible polarisation states. We will refer to them as longitudinally, left-handedly or right-handedly polarized W bosons. The net amount of polarisation is given by the fractions of the partial decay widths for differently polarised W bosons, Γ_0 , Γ_L and Γ_R , respectively. These “helicity fractions” are

$$F_{0/L/R} = \frac{\Gamma_{0/L/R}}{\Gamma_0 + \Gamma_L + \Gamma_R}.$$

In perturbation theory at LO, and neglecting the mass of the bottom quark, these fractions depend solely on the masses of the top quark and the W boson, i.e.

$$\begin{aligned}F_0 &= \frac{m_t^2}{m_t^2 + 2M_W^2} \approx 0.70, \\ F_L &= \frac{2M_W^2}{m_t^2 + 2M_W^2} \approx 0.30, \\ F_R &= 0.\end{aligned}$$

Calculations at NNLO that include electroweak corrections and assume a finite mass of the bottom quark yield $F_0 = 0.687 \pm 0.005$, $F_L = 0.311 \pm 0.005$ and $F_R = 0.0017 \pm 0.0001$ [124]. The helicity fractions can be altered if the structure of the Wtb vertex differs from a pure $V-A$ coupling. Such deviations are typically described by anomalous couplings in effective field theory approaches [125, 126].

Information about the polarisation of the W boson can be obtained from angular distributions of the final-state particles. In the single-lepton and dilepton channels of $t\bar{t}$ production, the angle θ^* is defined as the angle between the reverse momentum of the leptonically decaying top quark and the direction of the charged lepton, both evaluated in the rest frame of the corresponding W boson [127]. The differential decay width can then be written as

$$\begin{aligned}\frac{1}{\Gamma} \frac{d\Gamma}{d \cos(\theta^*)} &= \sin(\theta^*)^2 F_0 + \frac{3}{8} (1 - \cos(\theta^*))^2 F_L \\ &\quad + \frac{3}{8} (1 + \cos(\theta^*))^2 F_R.\end{aligned}\tag{5}$$

An angle for the hadronically decaying top quark can be defined analogously. The ATLAS and CMS collaborations have both made use of the angular dependence described by equation (5) to estimate the helicity fractions.

The ATLAS collaboration has analysed a data set corresponding to an integrated luminosity of 1.04 fb^{-1} taken at a centre-of-mass energy of $\sqrt{s} = 7 \text{ TeV}$ [128]. Two sets of selection criteria are defined so as to enrich samples with events stemming from $t\bar{t}$ production with subsequent decay either in the single-lepton or dilepton decay modes. In both cases, the reconstruction of the top quarks is based on the final-state particles and assumptions on the detector performance. For both event types, an individual analysis strategy is followed. While the first strategy is based on a template fit of the $\cos(\theta^*)$ distributions, the second makes use of the angular asymmetries derived from unfolded $\cos(\theta^*)$ spectra. The individual results are all found to be in agreement and are combined using the BLUE method [129]. Although both analysis methods are based on the same data set, the combined result has a smaller overall uncertainty due to the different sensitivities to sources of systematic uncertainty. The largest systematic uncertainties are due to the signal and background modelling, to the jet reconstruction and to method-specific uncertainties. The combined helicity fractions are

$$\begin{aligned} F_0 &= 0.67 \pm 0.03 \text{ (stat)} \pm 0.06 \text{ (syst)}, \\ F_L &= 0.32 \pm 0.02 \text{ (stat)} \pm 0.03 \text{ (syst)}, \\ F_R &= 0.01 \pm 0.01 \text{ (stat.)} \pm 0.04 \text{ (syst)}, \end{aligned}$$

with a correlation between F_0 and F_L of -0.96 .

The CMS collaboration has analysed the full 7 TeV data set corresponding to an integrated luminosity of 5.0 fb^{-1} [130]. Events are selected that are compatible with the single-lepton decay mode, and top quarks are reconstructed from the final-state particles using a constrained fit. An estimate of the helicity fractions is obtained using a reweighting procedure and a subsequent fit to the $\cos(\theta^*)$ distribution. The largest sources of systematic uncertainty are the background estimate and the jet reconstruction. The helicity fractions are estimated to be

$$\begin{aligned} F_0 &= 0.682 \pm 0.030 \text{ (stat)} \pm 0.033 \text{ (syst)}, \\ F_L &= 0.310 \pm 0.022 \text{ (stat)} \pm 0.022 \text{ (syst)}, \\ F_R &= 0.008 \pm 0.012 \text{ (stat)} \pm 0.014 \text{ (syst)}, \end{aligned}$$

with a correlation between F_0 and F_L of -0.95 . A more recent measurement of the helicity fractions using a data sample collected at $\sqrt{s} = 8 \text{ TeV}$ and enriched with single top-quark events is in good agreement with these values [131].

The results obtained by the ATLAS and CMS collaborations are consistent with one another and with the NNLO predictions. Both measurements are more precise than those published by Tevatron experiments.

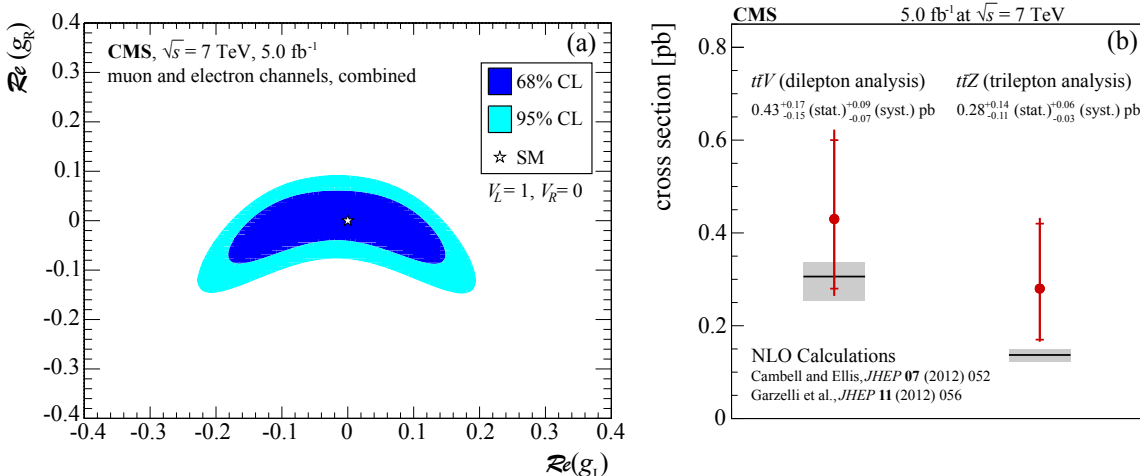


Fig. 19. (a) The 68% and 95% CL contours in the plane of the (real) tensor couplings g_R and g_L assuming vector couplings of $V_L = 1$ and $V_R = 0$ as obtained by the CMS collaboration. (b) Measured and predicted values of the cross sections for $t\bar{t}V$ and $t\bar{t}Z$ production. The inner and outer error bars indicate the statistical and total uncertainties, respectively. (*Adapted from Refs. [130, 132].*)

The measured helicity fractions are also interpreted in terms of anomalous couplings. Figure 19(a) shows the 68% and 95% CL contours in the plane of the (real) tensor couplings g_R and g_L assuming vector couplings of $V_L = 1$ and $V_R = 0$ as obtained by the more precise CMS result. A second region of solutions featuring large values of the real part of g_R is excluded from the fit as it is not compatible with the measurement of the single-top t -channel cross section. The results are consistent with the absence of anomalous couplings, i.e. $g_L = g_R = 0$, and are in very good agreement with the predicted $V-A$ structure of the Wtb vertex.

5.2 Top-Quark Pairs and Additional Gauge Bosons

While the production of a top-quark pair and an additional photon has only been observed at the Tevatron [133], the CMS collaboration was the first to measure the production of top-quark pairs with additional Z bosons ($t\bar{t}Z$) and W bosons ($t\bar{t}W$) [132, 134]. Such rare processes are expected in the SM. For a centre-of-mass energy of $\sqrt{s} = 7$ TeV, calculations at NLO yield predictions for the corresponding cross sections $\sigma_{t\bar{t}Z}$ [135] and $\sigma_{t\bar{t}W}$ [136] of

$$\begin{aligned}\sigma_{t\bar{t}Z} &= 0.137^{+0.012}_{-0.016} \text{ pb}, \\ \sigma_{t\bar{t}W} &= 0.169^{+0.029}_{-0.051} \text{ pb}.\end{aligned}$$

Here the analysis at $\sqrt{s} = 7$ TeV is briefly described [132]. The data set collected corresponds to an integrated luminosity of 5.0 fb^{-1} . Events are selected according to the number of charged leptons in the final state. The process

$$pp \rightarrow t\bar{t}Z \rightarrow (t \rightarrow b\ell^\pm\nu)(t \rightarrow bjj)(Z \rightarrow \ell^\pm\ell^\mp)$$

is searched for by requiring two leptons with the same flavour but opposite electric charge and with an invariant mass compatible with the mass of the Z boson, and one additional charged lepton. After the event selection, nine events are observed while 3.2 ± 0.8 background events are expected. The resulting cross section is estimated to be

$$\sigma_{t\bar{t}Z} = 0.28^{+0.14}_{-0.11} \text{ (stat)}^{+0.06}_{-0.03} \text{ (syst) pb},$$

where the dominant source of systematic uncertainty is the background yield.

On the other hand, the processes

$$\begin{aligned}pp \rightarrow t\bar{t}Z \rightarrow (t \rightarrow b\ell^\pm\nu)(t \rightarrow bjj)(Z \rightarrow \ell^\pm\ell^\mp), \text{ and} \\ pp \rightarrow t\bar{t}W \rightarrow (t \rightarrow b\ell^\pm\nu)(t \rightarrow bjj)(W \rightarrow \ell^\pm\nu)\end{aligned}$$

are searched for by selecting events with exactly two leptons of the same electric charge. After the event selection, 16 events remain, while the background expectation is 9.2 ± 2.6 . The combined cross section, $\sigma_{t\bar{t}V}$, where $V = W, Z$, is measured as

$$\sigma_{t\bar{t}V} = 0.43^{+0.17}_{-0.15} \text{ (stat)}^{+0.09}_{-0.07} \text{ (syst) pb}.$$

Both measurements and their NLO predictions are shown in figure 19(b). The measured cross sections are in agreement with the predictions, which indicates that no deviation from the strength of the top-quark coupling to Z and W bosons predicted by the SM is observed. The results from the more recent CMS analysis at $\sqrt{s} = 8$ TeV [134] are also consistent with this conclusion.

6 Single Top-Quark Production

Single top-quark production, in contrast to top-quark pair-production which proceeds through the strong interactions, takes place by virtue of charged-current interactions. The production rate for single top quarks is suppressed with respect to top-quark pair production by a factor of 2–3 due to the different couplings strengths α_W and α_s of weak and strong interactions, which is only partially compensated by the larger partonic fluxes due to the lower production threshold. Feynman diagrams of the LO processes contributing to the scattering amplitudes are shown in figure 20.

Depending on whether the W boson is space-like (figure 20(a)), time-like (figure 20(b)) or real (figure 20(c,d)), one distinguishes between the t -channel, the s -channel and the tW -channel. In the latter

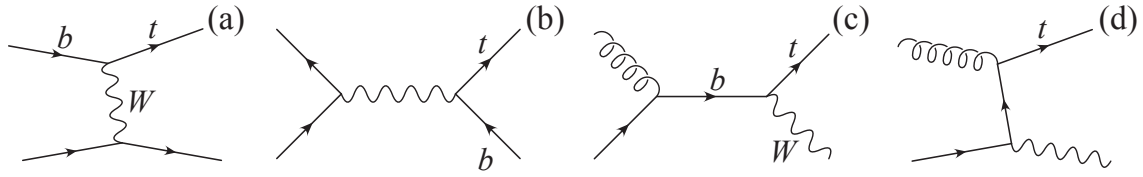


Fig. 20. Leading-order Feynman diagrams of processes contributing to single top-quark production: (a) t -channel, (b) s -channel, (c, d) tW -channel.

case, a single top quark is produced in association with a W boson in the final state. The dominant contribution to single top-quark production at the Tevatron and the LHC is the t -channel. As can be seen from figure 20(a), this channel assumes the existence of a b quark inside the proton and thus requires in the theoretical description the so-called five-flavour scheme, in which u, d, s, c, b are treated as active flavours inside the proton. In the four-flavour scheme, t -channel production occurs formally at higher orders of the QCD coupling, as is illustrated in figure 21. In general, calculations in these two schemes should give

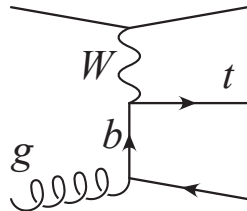


Fig. 21. Leading-order Feynman diagram for t -channel single top-quark production in the four-flavour scheme.

similar results. Differences occur if logarithmic corrections of the form $\ln(m_b^2/Q^2)$ become large, where Q denotes a generic energy scale. The five-flavour scheme may partially resum these logarithms through the evolution of the b -quark parton distribution function, while in the four-flavour scheme these logarithms are kept at fixed order only. In Refs. [137, 138] it has been checked through an explicit calculation that the two schemes lead indeed to consistent results for the cross section.

At the LHC, the second important production channel for single top quarks is the tW channel. Due to phase-space suppression and the small gluon luminosity, this channel gives only a tiny contribution at the Tevatron. In contrast, s -channel production, which is roughly responsible for one third of the cross section at the Tevatron, leads only to a contribution of a few percent at the LHC. Single top-quark production at the LHC is thus to some extent complementary to that at the Tevatron. A further major difference arises from the fact that the initial state at the Tevatron is a CP eigenstate. Since CP -violating effects are negligible in single top-quark production within the SM, the numbers of produced single top quarks and antiquarks are identical at the Tevatron. At the LHC, however, the initial state is not a CP eigenstate, and more top quarks than antiquarks are produced because in pp collisions the flux of up-type quarks is larger than the flux for down-type quarks.

The NLO QCD corrections for inclusive single top-quark production have been presented in Refs. [139–141] for the t -channel, in Ref. [142] for the s -channel and in Refs. [143, 144] for the tW channel.

| | LHC 8 TeV | | | | Tevatron | |
|------|------------------------|------------------------|--|--|----------------------------------|---|
| | σ_t^{LO} | σ_t^{LO} | σ_t^{NLO} | σ_t^{NLO} | $\sigma_{t,\bar{t}}^{\text{LO}}$ | $\sigma_{t,\bar{t}}^{\text{NLO}}$ |
| t | 53.8 | 29.1 | $55.2^{+1.6}_{-0.9}{}^{+0.35}_{-0.32}$ | $30.1^{+0.9}_{-0.5}{}^{+0.29}_{-0.32}$ | 1.03 | $0.998^{+0.025}_{-0.022}{}^{+0.029}_{-0.032}$ |
| s | 2.22 | 1.24 | $3.30^{+0.06}_{-0.08}{}^{+0.07}_{-0.05}$ | $1.90^{+0.04}_{-0.05}{}^{+0.04}_{-0.03}$ | 0.28 | $0.442^{+0.015}_{-0.023}{}^{+0.015}_{-0.011}$ |
| tW | 8.86 | 8.85 | $9.12^{+0.21}_{-0.38}{}^{+0.29}_{-0.36}$ | $9.11^{+0.21}_{-0.38}{}^{+0.29}_{-0.36}$ | 0.069 | $0.070^{+0.008}_{-0.001}{}^{+0.008}_{-0.009}$ |

Table 2. Cross sections for single top-quark production at LO and NLO QCD using $m_t = 173.3$ GeV and the MSTW2008lo/nlo PDF set. See text for references.

The notation is $\sigma(\mu = m_t) \frac{\sigma(\mu=2m_t) - \sigma(\mu=m_t)}{\sigma(\mu=\frac{m_t}{2}) - \sigma(\mu=m_t)} + \text{PDF err. up}$ – PDF err. down .

These cross sections are shown in table 2, assuming $m_t = 173.3$ GeV and using the MSTW2008lo/nlo68cl pdf set [27]. It turns out that the NLO corrections are only a few percent for the t -channel and slightly larger for the tW channel. In contrast, the NLO corrections to the s -channel contribution are about 30%. However, as has been pointed out before, this channel gives only a small contribution at the LHC. Since at NLO, no colour transfer between the two quark lines is allowed (the corresponding box contributions vanish after interference with the Born amplitude), it is conceivable that the small corrections are accidental and that the small scale uncertainty observed at NLO underestimates the possible size of the NNLO corrections. Very recently, the vertex corrections for the t -channel have been calculated at NNLO QCD [145]. The corrections are found to be comparable in size to the NLO corrections.

Fully differential results at NLO accuracy for single top-quark production have been presented in Refs. [146–148]. In Refs. [149–152], the analysis has been extended by including the semileptonic decay of the top quark in the narrow-width approximation. In addition, the systematic combination of the NLO corrections with the parton shower has been investigated in MC@NLO [153, 154] as well as in the POWHEG framework [155, 156]. Beyond fixed-order perturbation theory, the impact of logarithmic corrections due to soft-gluon emission has been studied [157–162].

As will be seen below, the experimental study of single top-quark production is challenging—despite the sizeable cross sections—because of the complicated event signature and the large backgrounds. In contrast to $t\bar{t}$ production, singly-produced top quarks are highly polarised—a consequence of their $V-A$ coupling to the W boson. The measurement of the top-quark polarisation thus provides a further test of the $V-A$ structure of the tWb vertex. Assuming that the production mechanism is well understood, t -channel single top-quark production can also be used to constrain the b parton distribution in the proton. Furthermore, it can be used for a direct measurement of the CKM matrix element V_{tb} which is otherwise only indirectly accessible, via the assumptions of CKM matrix unitarity and of the existence of only three quark families.

6.1 t -Channel Production

Measurements of the t -channel production cross section have been performed using events with exactly one isolated lepton (electron or muon) originating from the decay of the W boson and two or three jets in the final state. One of the jets has to be identified as a b jet. Additional requirements on kinematic observables, such as the missing transverse momentum or the transverse mass of the W boson, are imposed in order to further remove background. Detailed and precise results are available from ATLAS and CMS [163–167].

An early analysis of t -channel single-top production was performed by the ATLAS collaboration based on an integrated luminosity of about 1 fb^{-1} [163]. Events with two or three jets are selected. To separate t -channel single top-quark signal events from backgrounds, several kinematic variables are combined into one discriminant by employing a neural network that also exploits correlations between the variables. The most discriminating variable for the two-jet sample is the invariant mass of the system formed by the b -tagged jet, the charged lepton and the neutrino, $m_{\ell\nu b}$, see figure 22(a). In the three-jet category, the invariant mass of the two leading jets and the absolute value of the difference in pseudo-rapidity of the leading and the lowest- p_T jet are among the most discriminating variables. Multi-jet event yields are determined with data-driven techniques, while contributions from $W+\text{jets}$ events are derived from simulation and normalised to data in control regions using a cut-based analysis. All other backgrounds and the t -channel signal expectation are normalised to theoretical cross sections. To extract the signal content of the selected sample, a maximum-likelihood fit is performed to the output distributions of the neural net in the two-jet and three-jet data sets. From a simultaneous measurement in the two channels, a cross section of

$$\sigma_{t+\bar{t}} = 83 \pm 4 \text{ (stat)}^{+20}_{-19} \text{ (syst) pb}$$

is measured. This result is confirmed in a cut-based analysis which is illustrated by the distribution in figure 22(b).

More recently, the CMS collaboration performed an analysis based on the full statistics available for $\sqrt{s} = 8$ TeV [166]. The event sample is selected by the application of simple criteria: The events must contain exactly one muon or electron with large transverse momentum. They are categorised according to the numbers of jets and b -tagged jets, and the category enriched with t -channel signal is the one with two jets and one tag. One of the jets, denoted by j' , is expected to not originate from b quarks, and its pseudo-rapidity distribution is typical of the t -channel processes where a light parton recoils against a much more massive particle like the top quark. Signal events populate forward regions in the $|\eta_{j'}|$ spectrum, and this

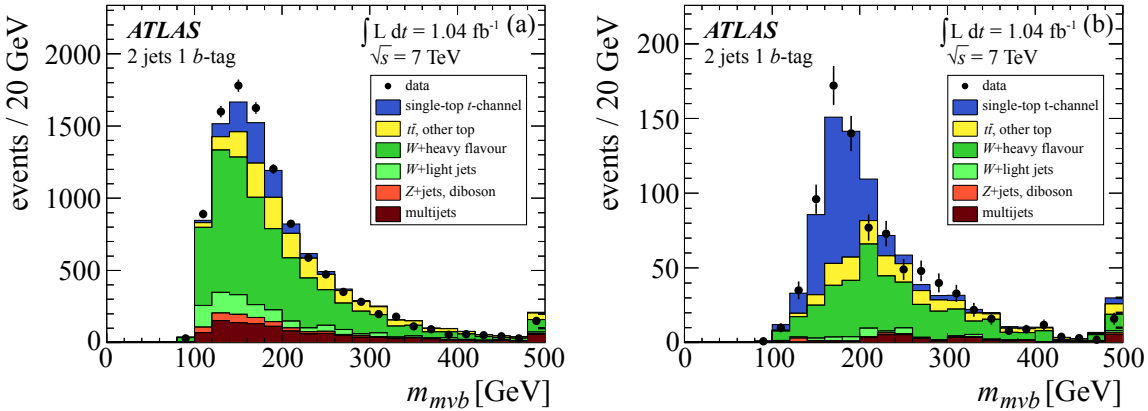


Fig. 22. Distribution of the invariant mass of the b -tagged jet, the charged lepton and the neutrino in the b -tagged sample for two-jet events (a) for the inclusive sample and (b) after cuts. The last histogram bin includes overflow. (Adapted from Ref. [163].)

feature is used to distinguish the signal from background. Background events from $t\bar{t}$ and from W +jets processes are determined by the use of control categories. In all categories the invariant mass $m_{\ell\nu b}$ is used to define a signal region and a side-band region that contain events inside and outside the reconstructed top-quark mass window of $130 < m_{\ell\nu b} < 220$ GeV, respectively. To determine the contribution from signal events, a binned maximum-likelihood fit is performed to the $|\eta_{j'}|$ distribution of the events in the signal region of the category with two jets and one tag. In figure 23 (a) the $m_{\ell\nu b}$ distribution is shown for events with forward jets. The figure illustrates that large-purity samples of t -channel single-top quark events can be isolated at the LHC using simple selection criteria. The measured cross section for this process is

$$\sigma_{t+\bar{t}} = 83.6 \pm 2.3 \text{ (stat)} \pm 7.4 \text{ (syst)} \text{ pb}.$$

The largest contributions to the systematic uncertainty come from the choice of the renormalisation and factorisation scales in the simulation of the signal samples and from uncertainties on the jet energy scale and resolutions. From another fit, the cross sections for t quarks and \bar{t} quarks and the corresponding ratio, $R_t = \sigma_t/\sigma_{\bar{t}}$, are obtained:

$$\begin{aligned} \sigma_t &= 53.8 \pm 4.4 \text{ (stat)} \pm 8 \text{ (syst)} \text{ pb}, \\ \sigma_{\bar{t}} &= 27.6 \pm 1.3 \text{ (stat.)} \pm 3.7 \text{ (syst)} \text{ pb}, \\ R_t &= 1.95 \pm 0.10 \text{ (stat)} \pm 0.19 \text{ (syst)}. \end{aligned}$$

In figure 23(b) the measured ratio is compared with predictions using different PDF sets.

The largeness of the LHC data samples and of the t -channel single top cross section give access to detailed studies of differential distributions [167] and properties, such as the top-quark polarisation, W helicity distributions, and mass measurements. At the time of preparation of this volume, the publication of the latter measurements is still in progress.

6.2 Single Top-Quark Production in Association with a W Boson

At the LHC, the production of single top quarks in association with W bosons becomes experimentally accessible for the first time. First evidence was reported by ATLAS using about the first half of the 7 TeV data recorded in 2011 [168] and was confirmed by CMS [169]. The ATLAS analysis makes use of dileptonic final states with events featuring two isolated leptons (electron or muon) with significant transverse missing momentum and at least one jet. A boosted decision tree (BDT) is used to discriminate single top-quark tW events from background events, which mostly arise from top-quark pair production. The result is extracted from a template fit to the BDT output discriminant distribution, which is shown in figure 24(a). It is incompatible with the background-only hypothesis at the 3.3σ level. The expected sensitivity assuming the Standard Model production rate is 3.4σ . The measured cross section is

$$\sigma_{tW} = 16.8 \pm 2.9 \text{ (stat)} \pm 4.9 \text{ (syst)} \text{ pb}.$$

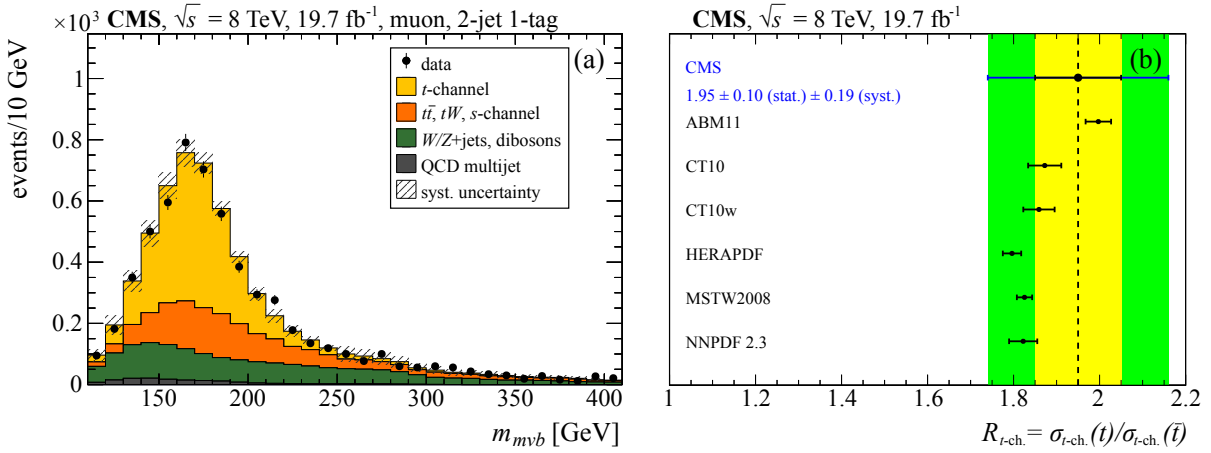


Fig. 23. (a) Distribution of the invariant mass $m_{\ell\nu b}$ for the muon decay channel in the region with $|\eta_j| > 2.5$ as measured by CMS. (b) Comparison of the measured t -channel top quark/antiquark production ratio with the predictions obtained using different PDF sets. (*Adapted from Refs. [166, 166].*)

The uncertainty of the jet energy scale and of the modelling of the production process are dominant sources of systematic uncertainty.

Most recently, the CMS collaboration reported an observation of the process based on 8 TeV data [170]. Similarly to previous analyses, a multivariate analysis technique makes use of kinematic and topological properties to separate the signal from the dominant $t\bar{t}$ background. An excess consistent with the signal hypothesis is observed, with an observed (expected) significance of 6.1 (5.4) standard deviations above a background-only hypothesis. In figure 24b the distribution of tW events over different event categories is shown. The measured production cross section is 23.4 ± 5.4 pb, in agreement with the Standard Model prediction.

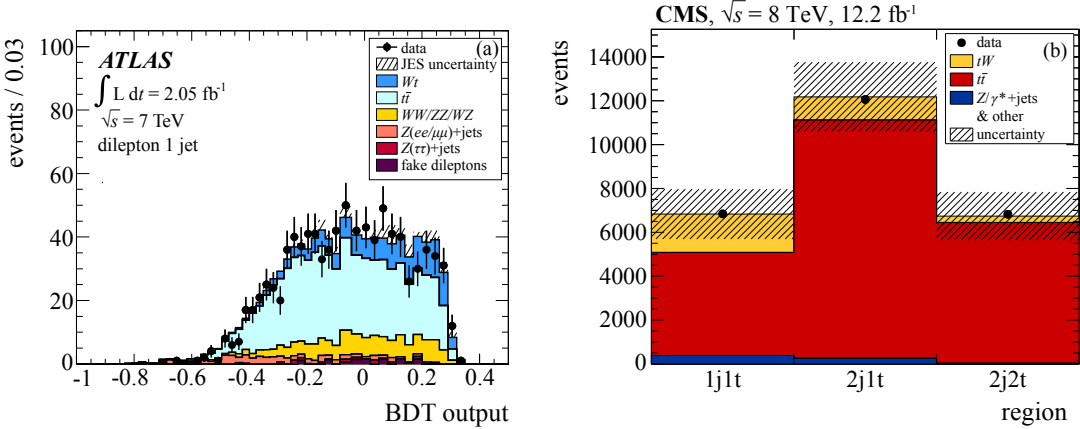


Fig. 24. (a) BDT output for selected events in the 1-jet category of the ATLAS analysis. The tW signal is normalised to the theory prediction. (b) Event yields in the signal region with one jet and one b -tagged jet (1j1t) and the control regions (2j1t and 2j2t) for the CMS analysis. The hatched band represents uncertainties of the predicted event yields. (*Adapted from Refs. [168, 170].*)

6.3 Determination of V_{tb}

Single top-quark production measurements also give access to the determination of the modulus of the CKM matrix element V_{tb} since in the SM t -channel and s -channel production depend on $|V_{tb}|^2$. The extraction is independent of assumptions about the number of quark generations and about the unitarity of

| Measurement | $ V_{tb} ^2$ | $ V_{tb} $ limit at 95% CL |
|------------------------|---|----------------------------|
| t -ch., ATLAS [167] | 1.02 ± 0.07 | > 0.88 |
| t -ch., CMS [166] | $0.998 \pm 0.038(\text{exp}) \pm 0.016(\text{theo})$ | > 0.92 |
| tW -ch., ATLAS [168] | $1.03^{+0.16}_{-0.19}$ | n/a |
| tW -ch., CMS [170] | $1.03 \pm 0.12(\text{exp}) \pm 0.04(\text{theo})$ | > 0.78 |
| R_B , CMS [171] | $1.014 \pm 0.003(\text{stat}) \pm 0.032(\text{syst})$ | > 0.975 |

Table 3. Most precise values and limits for $|V_{tb}|^2$ as extracted from single top-quark cross-section measurements and from R_B .

the CKM matrix. The only assumptions required are that $|V_{tb}| \gg |V_{ts}|, |V_{td}|$ and that the Wtb interaction is a SM-like left-handed weak coupling. Using the single-top cross section measurements, $|V_{tb}|^2$ can be extracted from a comparison of the measured and the predicted cross section. Assuming unitarity of the CKM matrix, $|V_{tb}| \leq 1$, a limit can be set. The most precise results are summarised in table 3.

A significantly more precise determination of V_{tb} can be obtained from the measurement of the ratio $R_B = B(t \rightarrow Wb)/B(t \rightarrow Wq)$. Measurements of R_B have also been performed at the Tevatron [172–174]. CMS presented a measurement of R_B using a binned-likelihood function of the observed b -tagging multiplicity distributions in events with two, three, or four observed jets in the different dilepton channels [171]. In figure 25 the variation of the profile likelihood ratio is shown. The fit yields a value $R_B = 1.014 \pm 0.003$ (stat) ± 0.032 (syst). Assuming the CKM matrix to be unitary, a lower limit for V_{tb} of 0.975 is set at the 95% confidence level.

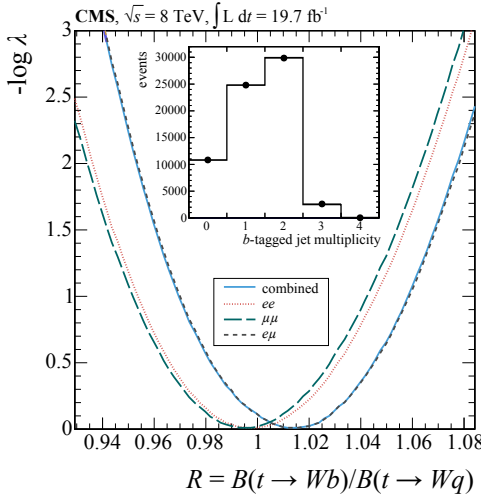


Fig. 25. Variations of the likelihood ratio used to extract R_B from the data. The variations observed in the combined fit and in the exclusive ee , $\mu\mu$, and $e\mu$ channels are shown separately. The inset shows the inclusive b -tagged jet multiplicity distribution and the fit distribution. (Adapted from Ref. [171].)

7 Conclusions

LHC data have brought a large boost to the field of top-quark physics, and since the LHC start in 2009, tremendous progress has been made.

On the theoretical side, a major breakthrough has been made with the calculation of the NNLO QCD corrections for inclusive production of top-quark pairs. Very recently, the theoretical calculations have been extended to include also predictions for differential distributions. The NNLO QCD corrections have been further improved by including weak corrections, the resummation of logarithmically enhanced contributions due to soft-gluon emission, and bound-state effects. In addition, finite-width effects have been studied in ground-breaking calculations by studying the one-loop QCD corrections including the decay of the top quark. For the experimental analysis, NLO predictions matched and merged to take into account parton-shower corrections and predictions for larger jet multiplicities are available. For

single-top-quark production, NLO QCD corrections are known including also the decay of the top quark. For t -channel production, the theoretical predictions have been extended recently to include also partial results at NNLO QCD. In addition, conceptual differences using four or five flavours in the initial state have been studied in detail. For many observables the theoretical uncertainties are at the level of ten percent, and in some cases even the level of a few percent is reached. Beyond the steadily improving quality of theoretical predictions, a variety of new observables that allow precise tests of the underlying theory have been proposed. New methods to measure the top-quark mass are currently under development.

On the experimental side, during LHC Run 1, a rich and diverse program of top-quark measurements and studies has been performed, yielding a comprehensive spectrum of detailed and precise results.

Many of the measurements previously carried out at the Tevatron have been repeated at the LHC, and in many areas the size of the LHC top-quark data samples has facilitated in-depth studies at unprecedented levels of precision. Detailed and precise measurements of differential top-quark cross sections have been performed at the LHC, providing new insights in the top-quark production process and in QCD. Precision measurements of top-quark properties have as yet confirmed the SM expectations. Some of these properties, such as the polarisation of top quarks, the correlation of the top-quark spins in pair production, or the production of top quarks with additional gauge bosons were measured at the LHC for the first time. Stringent limits were set on anomalous couplings, e.g. flavour-changing neutral currents in the top-quark sector.

To date, most LHC top-quark measurements are no longer limited by statistical, but by systematic uncertainties. The latter are related to both the detector and the modelling of top-quark production and decay. Prime examples for the former are the jet energy scale and b -tagging uncertainties, while examples for the latter include the modelling of initial-state and final-state radiation as well as scale and hadronisation uncertainties. Substantial effort is being invested to reduce these uncertainties, through auxiliary measurements, through tuning of Monte Carlo generators and through further improvements of the theoretical calculations. The wealth of the LHC Run 1 results is the avant-garde of many more exciting improvements in the future, both in precision measurements as well as in searches for rare processes associated with top quarks.

References

1. T. Schörner-Sadenius, ed., “The Large Hadron Collider — Harvest of Run 1”. Springer, Heidelberg, Germany, 2015.
2. M. Kobayashi and T. Maskawa, “CP Violation in the Renormalizable Theory of Weak Interaction”, *Prog. Theor. Phys.* **49** (1973) 652.
3. CDF Collaboration, “Observation of top quark production in $\bar{p}p$ collisions”, *Phys. Rev. Lett.* **74** (1995) 2626, [arXiv:hep-ex/9503002](https://arxiv.org/abs/hep-ex/9503002).
4. DØ Collaboration, “Observation of the top quark”, *Phys. Rev. Lett.* **74** (1995) 2632, [arXiv:hep-ex/9503003](https://arxiv.org/abs/hep-ex/9503003).
5. CDF and DØ Collaborations, “Combination of measurements of the top-quark pair production cross section from the Tevatron Collider”, *Phys. Rev. D* **89** (2014) 072001, [doi:10.1103/PhysRevD.89.072001](https://doi.org/10.1103/PhysRevD.89.072001), [arXiv:1309.7570](https://arxiv.org/abs/1309.7570).
6. Tevatron Electroweak Working Group, “Combination of CDF and DØ results on the mass of the quark using up to 9.7 fb^{-1} at the Tevatron”, [arXiv:1407.2682](https://arxiv.org/abs/1407.2682).
7. P. Nason, S. Dawson, and R. K. Ellis, “The Total Cross-Section for the Production of Heavy Quarks in Hadronic Collisions”, *Nucl. Phys. B* **303** (1988) 607.
8. W. Beenakker et al., “QCD Corrections to Heavy Quark Production in p anti-p Collisions”, *Phys. Rev. D* **40** (1989) 54.
9. S. Catani et al., “The Top cross-section in hadronic collisions”, *Phys. Lett. B* **378** (1996) 329, [arXiv:hep-ph/9602208](https://arxiv.org/abs/hep-ph/9602208).
10. R. Bonciani et al., “NLL resummation of the heavy quark hadroproduction cross-section”, *Nucl. Phys. B* **529** (1998) 424, [arXiv:hep-ph/9801375](https://arxiv.org/abs/hep-ph/9801375).
11. N. Kidonakis et al., “Sudakov resummation and finite order expansions of heavy quark hadroproduction cross-sections”, *Phys. Rev. D* **64** (2001) 114001, [arXiv:hep-ph/0105041](https://arxiv.org/abs/hep-ph/0105041).
12. N. Kidonakis and R. Vogt, “Next-to-next-to-leading order soft gluon corrections in top quark hadroproduction”, *Phys. Rev. D* **68** (2003) 114014, [arXiv:hep-ph/0308222](https://arxiv.org/abs/hep-ph/0308222).
13. S. Moch and P. Uwer, “Theoretical status and prospects for top-quark pair production at hadron colliders”, *Phys. Rev. D* **78** (2008) 034003, [arXiv:0804.1476](https://arxiv.org/abs/0804.1476).
14. M. Czakon and A. Mitov, “On the Soft-Gluon Resummation in Top Quark Pair Production at Hadron Colliders”, *Phys. Lett. B* **680** (2009) 154, [arXiv:0812.0353](https://arxiv.org/abs/0812.0353).

15. M. Cacciari et al., “Top-pair production at hadron colliders with next-to-next-to-leading logarithmic soft-gluon resummation”, *Phys. Lett. B* **710** (2012) 612, [arXiv:1111.5869](#).
16. M. Beneke et al., “Hadronic top-quark pair production with NNLL threshold resummation”, *Nucl. Phys. B* **855** (2012) 695, [arXiv:1109.1536](#).
17. K. Hagiwara, Y. Sumino, and H. Yokoya, “Bound-state Effects on Top Quark Production at Hadron Colliders”, *Phys. Lett. B* **666** (2008) 71, [arXiv:0804.1014](#).
18. Y. Kiyo et al., “Top-quark pair production near threshold at LHC”, *Eur. Phys. J. C* **60** (2009) 375, [arXiv:0812.0919](#).
19. W. Beenakker et al., “Electroweak one loop contributions to top pair production in hadron colliders”, *Nucl. Phys. B* **411** (1994) 343.
20. J. H. Kuhn, A. Scharf, and P. Uwer, “Electroweak corrections to top-quark pair production in quark-antiquark annihilation”, *Eur. Phys. J. C* **45** (2006) 139, [arXiv:hep-ph/0508092](#).
21. W. Bernreuther, M. Fuecker, and Z. Si, “Mixed QCD and weak corrections to top quark pair production at hadron colliders”, *Phys. Lett. B* **633** (2006) 54, [arXiv:hep-ph/0508091](#).
22. J. H. Kuhn, A. Scharf, and P. Uwer, “Electroweak effects in top-quark pair production at hadron colliders”, *Eur. Phys. J. C* **51** (2007) 37, [arXiv:hep-ph/0610335](#).
23. W. Bernreuther, M. Fuecker, and Z.-G. Si, “Weak interaction corrections to hadronic top quark pair production”, *Phys. Rev. D* **74** (2006) 113005, [arXiv:hep-ph/0610334](#).
24. W. Hollik and M. Kollar, “NLO QED contributions to top-pair production at hadron collider”, *Phys. Rev. D* **77** (2008) 014008, [arXiv:0708.1697](#).
25. W. Bernreuther, M. Fuecker, and Z.-G. Si, “Weak interaction corrections to hadronic top quark pair production: Contributions from quark-gluon and b anti-b induced reactions”, *Phys. Rev. D* **78** (2008) 017503, [arXiv:0804.1237](#).
26. M. Czakon, P. Fiedler, and A. Mitov, “Total Top-Quark Pair-Production Cross Section at Hadron Colliders Through $O(\alpha_S^4)$ ”, *Phys. Rev. Lett.* **110** (2013), no. 25, 252004, [arXiv:1303.6254](#).
27. A. Martin et al., “Parton distributions for the LHC”, *Eur. Phys. J. C* **63** (2009) 189, [arXiv:0901.0002](#).
28. J. M. Campbell and R. K. Ellis, “Top-quark processes at NLO in production and decay”, *J.Phys. G* **42** (2015) 015005, doi:10.1088/0954-3899/42/1/015005, [arXiv:1204.1513](#).
29. S. Frixione and B. R. Webber, “Matching NLO QCD computations and parton shower simulations”, *JHEP* **06** (2002) 029, [arXiv:hep-ph/0204244](#).
30. P. Nason, “A New method for combining NLO QCD with shower Monte Carlo algorithms”, *JHEP* **11** (2004) 040, [arXiv:hep-ph/0409146](#).
31. S. Frixione, P. Nason, and B. R. Webber, “Matching NLO QCD and parton showers in heavy flavor production”, *JHEP* **08** (2003) 007, [arXiv:hep-ph/0305252](#).
32. S. Frixione, P. Nason, and G. Ridolfi, “A Positive-weight next-to-leading-order Monte Carlo for heavy flavour hadroproduction”, *JHEP* **09** (2007) 126, [arXiv:0707.3088](#).
33. K. Melnikov and O. I. Yakovlev, “Final state interaction in the production of heavy unstable particles”, *Nucl. Phys. B* **471** (1996) 90, [arXiv:hep-ph/9501358](#).
34. A. Denner et al., “NLO QCD corrections to WWbb production at hadron colliders”, *Phys. Rev. Lett.* **106** (2011) 052001, [arXiv:1012.3975](#).
35. A. Denner et al., “NLO QCD corrections to off-shell top-antitop production with leptonic decays at hadron colliders”, *JHEP* **10** (2012) 110, [arXiv:1207.5018](#).
36. G. Bevilacqua et al., “Complete off-shell effects in top quark pair hadroproduction with leptonic decay at next-to-leading order”, *JHEP* **02** (2011) 083, [arXiv:1012.4230](#).
37. ATLAS Collaboration, “Measurement of the top quark-pair production cross section with ATLAS in pp collisions at $\sqrt{s} = 7$ TeV”, *Eur. Phys. J. C* **71** (2011) 1577, [arXiv:1012.1792](#).
38. CMS Collaboration, “First Measurement of the Cross Section for Top-Quark Pair Production in Proton-Proton Collisions at $\sqrt{s} = 7$ TeV”, *Phys. Lett. B* **695** (2011) 424, [arXiv:1010.5994](#).
39. ATLAS Collaboration, “Measurement of the top quark pair production cross-section with ATLAS in the single lepton channel”, *Phys. Lett. B* **711** (2012) 244, [arXiv:1201.1889](#).
40. ATLAS Collaboration, “Measurement of the top quark pair production cross section in pp collisions at $\sqrt{s} = 7$ TeV in dilepton final states with ATLAS”, *Phys. Lett. B* **707** (2012) 459, [arXiv:1108.3699](#).
41. CMS Collaboration, “Measurement of the $t\bar{t}$ production cross section and the top quark mass in the dilepton channel in pp collisions at $\sqrt{s} = 7$ TeV”, *JHEP* **07** (2011) 049, [arXiv:1105.5661](#).
42. CMS Collaboration, “Measurement of the Top-antitop Production Cross Section in pp Collisions at $\sqrt{s} = 7$ TeV using the Kinematic Properties of Events with Leptons and Jets”, *Eur. Phys. J. C* **71** (2011) 1721, [arXiv:1106.0902](#).

43. CMS Collaboration, “Measurement of the $t\bar{t}$ Production Cross Section in pp Collisions at 7 TeV in Lepton + Jets Events Using b -quark Jet Identification”, *Phys. Rev. D* **84** (2011) 092004, [arXiv:1108.3773](#).
44. ATLAS Collaboration, “Measurement of the $t\bar{t}$ production cross section in the tau+jets channel using the ATLAS detector”, *Eur. Phys. J. C* **73** (2013) 2328, [arXiv:1211.7205](#).
45. ATLAS Collaboration, “Measurement of the top quark pair cross section with ATLAS in pp collisions at $\sqrt{s} = 7$ TeV using final states with an electron or a muon and a hadronically decaying τ lepton”, *Phys. Lett. B* **717** (2012) 89, [arXiv:1205.2067](#).
46. ATLAS Collaboration, “Measurement of the cross section for top-quark pair production in pp collisions at $\sqrt{s} = 7$ TeV with the ATLAS detector using final states with two high-pt leptons”, *JHEP* **05** (2012) 059, [arXiv:1202.4892](#).
47. CMS Collaboration, “Measurement of the $t\bar{t}$ production cross section in pp collisions at $\sqrt{s} = 7$ TeV with lepton + jets final states”, *Phys. Lett. B* **720** (2013) 83, [arXiv:1212.6682](#).
48. CMS Collaboration, “Measurement of the $t\bar{t}$ production cross section in the dilepton channel in pp collisions at $\sqrt{s} = 7$ TeV”, *JHEP* **11** (2012) 067, [arXiv:1208.2671](#).
49. CMS Collaboration, “Measurement of the $t\bar{t}$ production cross section in the all-jet final state in pp collisions at $\sqrt{s} = 7$ TeV”, *JHEP* **05** (2013) 065, [arXiv:1302.0508](#).
50. CMS Collaboration, “Measurement of the top-antitop production cross section in the tau+jets channel in pp collisions at $\sqrt{s} = 7$ TeV”, *Eur. Phys. J. C* **73** (2013) 2386, [arXiv:1301.5755](#).
51. CMS Collaboration, “Measurement of the top quark pair production cross section in pp collisions at $\sqrt{s} = 7$ TeV in dilepton final states containing a τ ”, *Phys. Rev. D* **85** (2012) 112007, [arXiv:1203.6810](#).
52. CMS Collaboration, “Measurement of the $t\bar{t}$ production cross section in pp collisions at $\sqrt{s} = 8$ TeV in dilepton final states containing one τ lepton”, *Phys. Lett. B* **739** (2014) 23, doi:[10.1016/j.physletb.2014.10.032](#), [arXiv:1407.6643](#).
53. ATLAS Collaboration, “Simultaneous measurements of the $t\bar{t}$, W^+W^- , and $Z/\gamma^* \rightarrow \tau\tau$ production cross-sections in pp collisions at $\sqrt{s} = 7$ TeV with the ATLAS detector”, [arXiv:1407.0573](#).
54. ATLAS Collaboration, “Measurement of the $t\bar{t}$ production cross-section using $e\mu$ events with b -tagged jets in pp collisions at $\sqrt{s} = 7$ and 8 TeV with the ATLAS detector”, *Eur. Phys. J. C* **74** (2014) 3109, doi:[10.1140/epjc/s10052-014-3109-7](#), [arXiv:1406.5375](#).
55. CMS Collaboration, “Measurement of the $t\bar{t}$ production cross section in the dilepton channel in pp collisions at $\sqrt{s} = 8$ TeV”, *JHEP* **02** (2014) 024, [arXiv:1312.7582](#).
56. P. Uwer and W. Wagner, “Top Quarks: The Peak of the Mass Hierarchy? in “Physics at the Terascale”, eds. Brock, I. and Schörner-Sadenius, T.”, pp. 187–209. Wiley-VCH, Weinheim (Germany), 2011.
57. ATLAS Collaboration, “Measurements of top quark pair relative differential cross-sections with ATLAS in pp collisions at $\sqrt{s} = 7$ TeV”, *Eur. Phys. J. C* **73** (2013) 2261, [arXiv:1207.5644](#).
58. CMS Collaboration, “Measurement of differential top-quark pair production cross sections in pp collisions at $\sqrt{s} = 7$ TeV”, *Eur. Phys. J. C* **73** (2013) 2339, [arXiv:1211.2220](#).
59. ATLAS Collaboration, “Measurements of normalized differential cross-sections for $t\bar{t}$ production in pp collisions at $\sqrt{s}=7$ TeV using the ATLAS detector”, *Phys. Rev. D* **90** (2014) 072004, doi:[10.1103/PhysRevD.90.072004](#), [arXiv:1407.0371](#).
60. S. Dittmaier, P. Uwer, and S. Weinzierl, “Hadronic top-quark pair production in association with a hard jet at next-to-leading order QCD: Phenomenological studies for the Tevatron and the LHC”, *Eur. Phys. J. C* **59** (2009) 625, [arXiv:0810.0452](#).
61. S. Alioli et al., “A new observable to measure the top-quark mass at hadron colliders”, *Eur. Phys. J. C* **73** (2013) 2438, [arXiv:1303.6415](#).
62. J. Alwall et al., “MadGraph 5 : Going Beyond”, *JHEP* **06** (2011) 128, doi:[10.1007/JHEP06\(2011\)128](#), [arXiv:1106.0522](#).
63. S. Dittmaier, P. Uwer, and S. Weinzierl, “NLO QCD corrections to t anti-t + jet production at hadron colliders”, *Phys. Rev. Lett.* **98** (2007) 262002, [arXiv:hep-ph/0703120](#).
64. S. Catani and M. Seymour, “A General algorithm for calculating jet cross-sections in NLO QCD”, *Nucl. Phys. B* **485** (1997) 291, [arXiv:hep-ph/9605323](#).
65. S. Catani et al., “The Dipole formalism for next-to-leading order QCD calculations with massive partons”, *Nucl. Phys. B* **627** (2002) 189, [arXiv:hep-ph/0201036](#).
66. K. Melnikov and M. Schulze, “NLO QCD corrections to top quark pair production in association with one hard jet at hadron colliders”, *Nucl. Phys. B* **840** (2010) 129, [arXiv:1004.3284](#).
67. K. Melnikov, A. Scharf, and M. Schulze, “Top quark pair production in association with a jet: QCD corrections and jet radiation in top quark decays”, *Phys. Rev. D* **85** (2012) 054002,

- [arXiv:1111.4991](#).
68. K. Melnikov, M. Schulze, and A. Scharf, “QCD corrections to top quark pair production in association with a photon at hadron colliders”, *Phys. Rev. D* **83** (2011) 074013, [arXiv:1102.1967](#).
 69. J. Pumplin et al., “New generation of parton distributions with uncertainties from global QCD analysis”, *JHEP* **07** (2002) 012, [arXiv:hep-ph/0201195](#).
 70. A. Bredenstein et al., “NLO QCD corrections to $pp \rightarrow t\bar{t}\text{bar} + X$ at the LHC”, *Phys. Rev. Lett.* **103** (2009) 012002, [arXiv:0905.0110](#).
 71. A. Bredenstein et al., “NLO QCD corrections to t anti-t b anti-b production at the LHC: 1. Quark-antiquark annihilation”, *JHEP* **08** (2008) 108, [arXiv:0807.1248](#).
 72. A. Bredenstein et al., “NLO QCD Corrections to Top Anti-Top Bottom Anti-Bottom Production at the LHC: 2. full hadronic results”, *JHEP* **03** (2010) 021, [arXiv:1001.4006](#).
 73. G. Bevilacqua et al., “Hadronic top-quark pair production in association with two jets at Next-to-Leading Order QCD”, *Phys. Rev. D* **84** (2011) 114017, [arXiv:1108.2851](#).
 74. G. Bevilacqua and M. Worek, “Constraining BSM Physics at the LHC: Four top final states with NLO accuracy in perturbative QCD”, *JHEP* **07** (2012) 111, [arXiv:1206.3064](#).
 75. S. Hoeche et al., “Next-to-leading order QCD predictions for top-quark pair production with up to two jets merged with a parton shower”, [arXiv:1402.6293](#).
 76. CMS Collaboration, “Measurement of jet multiplicity distributions in $t\bar{t}$ production in pp collisions at $\sqrt{s} = 7\text{ TeV}$ ”, *Eur. Phys. J. C* **74** (2014) 3014, doi:[10.1140/epjc/s10052-014-3014-0](#), [arXiv:1404.3171](#).
 77. ATLAS Collaboration, “Measurement of $t\bar{t}$ production with a veto on additional central jet activity in pp collisions at $\sqrt(s) = 7\text{ TeV}$ using the ATLAS detector”, *Eur. Phys. J. C* **72** (2012) 2043, [arXiv:1203.5015](#).
 78. ATLAS Collaboration, “Measurement of the $t\bar{t}$ production cross-section as a function of jet multiplicity and jet transverse momentum in 7 TeV proton-proton collisions with the ATLAS detector”, *JHEP* **1501** (2015) 020, doi:[10.1007/JHEP01\(2015\)020](#), [arXiv:1407.0891](#).
 79. ATLAS Collaboration, “Study of heavy-flavor quarks produced in association with top-quark pairs at $\sqrt{s} = 7\text{ TeV}$ using the ATLAS detector”, *Phys. Rev. D* **89** (2014) 072012, doi:[10.1103/PhysRevD.89.072012](#), [arXiv:1304.6386](#).
 80. S. Heinemeyer, W. Hollik, G. Weiglein, and L. Zeune, “Implications of LHC search results on the W boson mass prediction in the MSSM”, *JHEP* **12** (2013) 084, doi:[10.1007/JHEP12\(2013\)084](#), [arXiv:1311.1663](#).
 81. G. Degrassi et al., “Higgs mass and vacuum stability in the Standard Model at NNLO”, *JHEP* **1208** (2012) 098, doi:[10.1007/JHEP08\(2012\)098](#), [arXiv:1205.6497](#).
 82. G. Degrassi, “The role of the top quark in the stability of the SM Higgs potential”, *Nuovo Cim. C* **37** (2014) 47, doi:[10.1393/ncc/i2014-11735-1](#), [arXiv:1405.6852](#).
 83. A. Buckley et al., “General-purpose event generators for LHC physics”, *Phys. Rept.* **504** (2011) 145, doi:[10.1016/j.physrep.2011.03.005](#), [arXiv:1101.2599](#).
 84. S. Moch et al., “High precision fundamental constants at the TeV scale”, [arXiv:1405.4781](#).
 85. I. I. Y. Bigi et al., “The Pole mass of the heavy quark. Perturbation theory and beyond”, *Phys. Rev. D* **50** (1994) 2234, [arXiv:hep-ph/9402360](#).
 86. M. Beneke and V. M. Braun, “Heavy quark effective theory beyond perturbation theory: Renormalons, the pole mass and the residual mass term”, *Nucl. Phys. B* **426** (1994) 301, [arXiv:hep-ph/9402364](#).
 87. ATLAS Collaboration, “Measurement of the top quark mass with the template method in the $t\bar{t}$ - i lepton + jets channel using ATLAS data”, *Eur. Phys. J. C* **72** (2012) 2046, [arXiv:1203.5755](#).
 88. CMS Collaboration, “Measurement of the top-quark mass in $t\bar{t}$ events with dilepton final states in pp collisions at $\sqrt{s} = 7\text{ TeV}$ ”, *Eur. Phys. J. C* **72** (2012) 2202, [arXiv:1209.2393](#).
 89. CMS Collaboration, “Measurement of masses in the $t\bar{t}$ system by kinematic endpoints in pp collisions at $\sqrt{s} = 7\text{ TeV}$ ”, *Eur. Phys. J. C* **73** (2013) 2494, [arXiv:1304.5783](#).
 90. CMS Collaboration, “Measurement of the top-quark mass in all-jets $t\bar{t}$ events in pp collisions at $\sqrt{s}=7\text{ TeV}$ ”, *Eur. Phys. J. C* **74** (2014) 2758, doi:[10.1140/epjc/s10052-014-2758-x](#), [arXiv:1307.4617](#).
 91. CMS Collaboration, “Measurement of the top-quark mass in $t\bar{t}$ events with lepton+jets final states in pp collisions at $\sqrt{s} = 7\text{ TeV}$ ”, *JHEP* **12** (2012) 105, [arXiv:1209.2319](#).
 92. ATLAS Collaboration, “Measurement of the top-quark mass in the fully hadronic decay channel from ATLAS data at $\sqrt{s} = 7\text{ TeV}$ ”, [arXiv:1409.0832](#).

93. CMS Collaboration, “Measurement of the mass difference between top and antitop quarks”, *JHEP* **06** (2012) 109, [arXiv:1204.2807](#).
94. ATLAS Collaboration, “Measurement of the mass difference between top and anti-top quarks in pp collisions at $\sqrt{s} = 7$ TeV using the ATLAS detector”, *Phys. Lett. B* **728** (2014) 363, [arXiv:1310.6527](#).
95. ATLAS Collaboration, CDF Collaboration, CMS Collaboration, DØ Collaboration, “First combination of Tevatron and LHC measurements of the top-quark mass”, [arXiv:1403.4427](#).
96. CMS Collaboration, “Determination of the top-quark pole mass and strong coupling constant from the $t\bar{t}$ production cross section in pp collisions at $\sqrt{s} = 7$ TeV”, *Phys. Lett. B* **728** (2014) 496, doi:[10.1016/j.physletb.2014.08.040](#), [10.1016/j.physletb.2013.12.009](#), [arXiv:1307.1907](#).
97. J. H. Kuhn and G. Rodrigo, “Charge asymmetry in hadroproduction of heavy quarks”, *Phys. Rev. Lett.* **81** (1998) 49, [arXiv:hep-ph/9802268](#).
98. J. H. Kuhn and G. Rodrigo, “Charge asymmetry of heavy quarks at hadron colliders”, *Phys. Rev. D* **59** (1999) 054017, [arXiv:hep-ph/9807420](#).
99. W. Bernreuther and Z.-G. Si, “Top quark and leptonic charge asymmetries for the Tevatron and LHC”, *Phys. Rev. D* **86** (2012) 034026, [arXiv:1205.6580](#).
100. CDF Collaboration, “Measurement of the top quark forward-backward production asymmetry and its dependence on event kinematic properties”, *Phys. Rev. D* **87** (2013) 092002, [arXiv:1211.1003](#).
101. DØ Collaboration, “Forward-backward asymmetry in top quark-antiquark production”, *Phys. Rev. D* **84** (2011) 112005, [arXiv:1107.4995](#).
102. ATLAS Collaboration, “Measurement of the top quark pair production charge asymmetry in proton-proton collisions at $\sqrt{s} = 7$ TeV using the ATLAS detector”, *JHEP* **02** (2014) 107, [arXiv:1311.6724](#).
103. ATLAS Collaboration, “Measurement of the charge asymmetry in top quark pair production in pp collisions at $\sqrt{s} = 7$ TeV using the ATLAS detector”, *Eur. Phys. J. C* **72** (2012) 2039, [arXiv:1203.4211](#).
104. J. Erdmann et al., “A likelihood-based reconstruction algorithm for top-quark pairs and the KLFitter framework”, *Nucl. Instrum. Meth. A* **748** (2014) 18, doi:[10.1016/j.nima.2014.02.029](#), [arXiv:1312.5595](#).
105. G. Choudalakis, “Fully Bayesian Unfolding”, [arXiv:1201.4612](#).
106. CMS Collaboration, “Measurement of the charge asymmetry in top-quark pair production in proton-proton collisions at $\sqrt{s} = 7$ TeV”, *Phys. Lett. B* **709** (2012) 28, [arXiv:1112.5100](#).
107. CMS Collaboration, “Inclusive and differential measurements of the $t\bar{t}$ charge asymmetry in proton-proton collisions at 7 TeV”, *Phys. Lett. B* **717** (2012) 129, [arXiv:1207.0065](#).
108. V. Blobel, “An Unfolding method for high-energy physics experiments”, [arXiv:hep-ex/0208022](#).
109. CMS Collaboration, “Measurements of the $t\bar{t}$ charge asymmetry using the dilepton decay channel in pp collisions at $\sqrt{s} = 7$ TeV”, *JHEP* **04** (2014) 191, doi:[10.1007/JHEP04\(2014\)191](#), [arXiv:1402.3803](#).
110. A. Hocker and V. Kartvelishvili, “SVD approach to data unfolding”, *Nucl. Instrum. Meth. A* **372** (1996) 469, [arXiv:hep-ph/9509307](#).
111. Y. Grossman and I. Nachshon, “Hadronization, spin, and lifetimes”, *JHEP* **07** (2008) 016, [arXiv:0803.1787](#).
112. G. Mahlon and S. J. Parke, “Spin Correlation Effects in Top Quark Pair Production at the LHC”, *Phys. Rev. D* **81** (2010) 074024, [arXiv:1001.3422](#).
113. A. Brandenburg, Z. Si, and P. Uwer, “QCD corrected spin analyzing power of jets in decays of polarized top quarks”, *Phys. Lett. B* **539** (2002) 235, [arXiv:hep-ph/0205023](#).
114. W. Bernreuther, A. Brandenburg, and P. Uwer, “Transverse polarization of top quark pairs at the Tevatron and the large hadron collider”, *Phys. Lett. B* **368** (1996) 153, doi:[10.1016/0370-2693\(95\)01475-6](#), [arXiv:hep-ph/9510300](#).
115. W. G. Dharmaratna and G. R. Goldstein, “Gluon Fusion as a Source for Massive Quark Polarization”, *Phys. Rev. D* **41** (1990) 1731, doi:[10.1103/PhysRevD.41.1731](#).
116. W. Bernreuther and Z.-G. Si, “Top quark spin correlations and polarization at the LHC: standard model predictions and effects of anomalous top chromo moments”, *Phys. Lett. B* **725** (2013) 115, [arXiv:1305.2066](#).
117. W. Bernreuther and Z.-G. Si, “Distributions and correlations for top quark pair production and decay at the Tevatron and LHC.”, *Nucl. Phys. B* **837** (2010) 90, [arXiv:1003.3926](#).
118. DØ Collaboration, “Evidence for spin correlation in $t\bar{t}$ production”, *Phys. Rev. Lett.* **108** (2012) 032004, [arXiv:1110.4194](#).

119. ATLAS Collaboration, “Observation of spin correlation in $t\bar{t}$ events from pp collisions at $\sqrt{s} = 7$ TeV using the ATLAS detector”, *Phys. Rev. Lett.* **108** (2012) 212001, [arXiv:1203.4081](#).
120. ATLAS Collaboration, “Measurements of spin correlation in top-antitop quark events from proton-proton collisions at $\sqrt{s} = 7$ TeV using the ATLAS detector”, [arXiv:1407.4314](#).
121. CMS Collaboration, “Measurements of $t\bar{t}$ spin correlations and top-quark polarization using dilepton final states in pp collisions at $\sqrt{s} = 7$ TeV”, *Phys. Rev. Lett.* **112** (2014) 182001, [doi:10.1103/PhysRevLett.112.182001](#), [arXiv:1311.3924](#).
122. ATLAS Collaboration, “Measurement of Top Quark Polarization in Top-Antitop Events from Proton-Proton Collisions at $\sqrt{s} = 7$ TeV Using the ATLAS Detector”, *Phys. Rev. Lett.* **111** (2013) 232002, [doi:10.1103/PhysRevLett.111.232002](#), [arXiv:1307.6511](#).
123. DØ Collaboration, “Measurement of the top quark mass using dilepton events”, *Phys. Rev. Lett.* **80** (1998) 2063, [arXiv:hep-ex/9706014](#).
124. A. Czarnecki, J. G. Korner, and J. H. Piclum, “Helicity fractions of W bosons from top quark decays at NNLO in QCD”, *Phys. Rev. D* **81** (2010) 111503, [arXiv:1005.2625](#).
125. J. Aguilar-Saavedra et al., “Probing anomalous Wtb couplings in top pair decays”, *Eur. Phys. J. C* **50** (2007) 519, [arXiv:hep-ph/0605190](#).
126. C. Zhang and S. Willenbrock, “Effective-Field-Theory Approach to Top-Quark Production and Decay”, *Phys. Rev. D* **83** (2011) 034006, [arXiv:1008.3869](#).
127. G. L. Kane, G. Ladinsky, and C. Yuan, “Using the Top Quark for Testing Standard Model Polarization and CP Predictions”, *Phys. Rev. D* **45** (1992) 124.
128. ATLAS Collaboration, “Measurement of the W boson polarization in top quark decays with the ATLAS detector”, *JHEP* **06** (2012) 088, [arXiv:1205.2484](#).
129. A. Valassi, “Combining correlated measurements of several different physical quantities”, *Nucl. Instrum. Meth. A* **500** (2003) 391.
130. CMS Collaboration, “Measurement of the W-boson helicity in top-quark decays from $t\bar{t}$ production in lepton+jets events in pp collisions at $\sqrt{s} = 7$ TeV”, *JHEP* **10** (2013) 167, [arXiv:1308.3879](#).
131. CMS Collaboration, “Measurement of the W boson helicity in events with a single reconstructed top quark in pp collisions at $\sqrt{s} = 8$ TeV”, *JHEP* **1501** (2015) 053, [doi:10.1007/JHEP01\(2015\)053](#), [arXiv:1410.1154](#).
132. CMS Collaboration, “Measurement of associated production of vector bosons and top quark-antiquark pairs at $\sqrt{s} = 7$ TeV”, *Phys. Rev. Lett.* **110** (2013) 172002, [arXiv:1303.3239](#).
133. CDF Collaboration, “Evidence for $t\bar{t}\gamma$ Production and Measurement of $\sigma_{t\bar{t}\gamma}/\sigma_{t\bar{t}}$ ”, *Phys. Rev. D* **84** (2011) 031104, [arXiv:1106.3970](#).
134. CMS Collaboration, “Measurement of top quark-antiquark pair production in association with a W or Z boson in pp collisions at $\sqrt{s} = 8$ TeV”, *Eur. Phys. J. C* **74** (2014) 3060, [doi:10.1140/epjc/s10052-014-3060-7](#), [arXiv:1406.7830](#).
135. M. Garzelli et al., “ $t\bar{t}W^{+-}$ and $t\bar{t}Z$ Hadroproduction at NLO accuracy in QCD with Parton Shower and Hadronization effects”, *JHEP* **11** (2012) 056, [arXiv:1208.2665](#).
136. J. M. Campbell and R. K. Ellis, “ $t\bar{t}W^{+-}$ production and decay at NLO”, *JHEP* **07** (2012) 052, [arXiv:1204.5678](#).
137. J. M. Campbell et al., “Single-Top Production at Hadron Colliders”, *Phys. Rev. Lett.* **102** (2009) 182003, [arXiv:0903.0005](#).
138. J. Campbell et al., “NLO Predictions for t -Channel Production of Single Top and Fourth Generation Quarks at Hadron Colliders”, *JHEP* **10** (2009) 042, [arXiv:0907.3933](#).
139. G. Bordes and B. van Eijk, “Calculating QCD corrections to single top production in hadronic interactions”, *Nucl. Phys. B* **435** (1995) 23.
140. T. Stelzer, Z. Sullivan, and S. Willenbrock, “Single top quark production via W - gluon fusion at next-to-leading order”, *Phys. Rev. D* **56** (1997) 5919, [arXiv:hep-ph/9705398](#).
141. T. Stelzer, Z. Sullivan, and S. Willenbrock, “Single top quark production at hadron colliders”, *Phys. Rev. D* **58** (1998) 094021, [arXiv:hep-ph/9807340](#).
142. M. C. Smith and S. Willenbrock, “QCD and Yukawa corrections to single top quark production via $q\bar{q} \rightarrow tb$ ”, *Phys. Rev. D* **54** (1996) 6696, [arXiv:hep-ph/9604223](#).
143. W. T. Giele, S. Keller, and E. Laenen, “QCD corrections to W boson plus heavy quark production at the Tevatron”, *Phys. Lett. B* **372** (1996) 141, [arXiv:hep-ph/9511449](#).
144. S. Zhu, “Next-to-leading order QCD corrections to $b g \rightarrow t W^-$ at the CERN Large Hadron Collider”, *Phys. Lett. B* **524** (2002) 283.
145. M. Brucherseifer, F. Caola, and K. Melnikov, “On the NNLO QCD corrections to single-top production at the LHC”, *Phys. Lett. B* **736** (2014) 58–63,

- [doi:10.1016/j.physletb.2014.06.075](https://doi.org/10.1016/j.physletb.2014.06.075), arXiv:1404.7116.
146. B. Harris et al., “The Fully differential single top quark cross-section in next to leading order QCD”, *Phys. Rev. D* **66** (2002) 054024, arXiv:hep-ph/0207055.
 147. Z. Sullivan, “Understanding single-top-quark production and jets at hadron colliders”, *Phys. Rev. D* **70** (2004) 114012, arXiv:hep-ph/0408049.
 148. Z. Sullivan, “Angular correlations in single-top-quark and Wjj production at next-to-leading order”, *Phys. Rev. D* **72** (2005) 094034, arXiv:hep-ph/0510224.
 149. J. M. Campbell, R. K. Ellis, and F. Tramontano, “Single top production and decay at next-to-leading order”, *Phys. Rev. D* **70** (2004) 094012, arXiv:hep-ph/0408158.
 150. Q.-H. Cao and C.-P. Yuan, “Single top quark production and decay at next-to-leading order in hadron collision”, *Phys. Rev. D* **71** (2005) 054022, arXiv:hep-ph/0408180.
 151. Q.-H. Cao et al., “Next-to-leading order corrections to single top quark production and decay at the Tevatron: 2. t^- channel process”, *Phys. Rev. D* **72** (2005) 094027, arXiv:hep-ph/0504230.
 152. J. M. Campbell and F. Tramontano, “Next-to-leading order corrections to Wt production and decay”, *Nucl. Phys. B* **726** (2005) 109, arXiv:hep-ph/0506289.
 153. S. Frixione et al., “Single-top production in MC@NLO”, *JHEP* **03** (2006) 092, arXiv:hep-ph/0512250.
 154. S. Frixione et al., “Single-top hadroproduction in association with a W boson”, *JHEP* **07** (2008) 029, arXiv:0805.3067.
 155. S. Alioli et al., “NLO single-top production matched with shower in POWHEG: s- and t-channel contributions”, *JHEP* **09** (2009) 111, arXiv:0907.4076.
 156. E. Re, “Single-top Wt-channel production matched with parton showers using the POWHEG method”, *Eur. Phys. J. C* **71** (2011) 1547, arXiv:1009.2450.
 157. S. Mrenna and C. Yuan, “Effects of QCD resummation on W+ h and t anti-b production at the Tevatron”, *Phys. Lett. B* **416** (1998) 200, arXiv:hep-ph/9703224.
 158. N. Kidonakis, “Single top production at the Tevatron: Threshold resummation and finite-order soft gluon corrections”, *Phys. Rev. D* **74** (2006) 114012, arXiv:hep-ph/0609287.
 159. N. Kidonakis, “Higher-order soft gluon corrections in single top quark production at the LHC”, *Phys. Rev. D* **75** (2007) 071501, arXiv:hep-ph/0701080.
 160. N. Kidonakis, “Two-loop soft anomalous dimensions for single top quark associated production with a W- or H-”, *Phys. Rev. D* **82** (2010) 054018, arXiv:1005.4451.
 161. N. Kidonakis, “Next-to-next-to-leading soft-gluon corrections for the top quark cross section and transverse momentum distribution”, *Phys. Rev. D* **82** (2010) 114030, arXiv:1009.4935.
 162. N. Kidonakis, “Next-to-next-to-leading-order collinear and soft gluon corrections for t-channel single top quark production”, *Phys. Rev. D* **83** (2011) 091503, arXiv:1103.2792.
 163. ATLAS Collaboration, “Measurement of the t-channel single top-quark production cross section in pp collisions at $\sqrt{s} = 7$ TeV with the ATLAS detector”, *Phys. Lett. B* **717** (2012) 330, arXiv:1205.3130.
 164. CMS Collaboration, “Measurement of the t-channel single top quark production cross section in pp collisions at $\sqrt{s} = 7$ TeV”, *Phys. Rev. Lett.* **107** (2011) 091802, arXiv:1106.3052.
 165. CMS Collaboration, “Measurement of the single-top-quark t-channel cross section in pp collisions at $\sqrt{s} = 7$ TeV”, *JHEP* **12** (2012) 035, arXiv:1209.4533.
 166. CMS Collaboration, “Measurement of the t-channel single-top-quark production cross section and of the $|V_{tb}|$ CKM matrix element in pp collisions at $\sqrt{s}= 8$ TeV”, *JHEP* **06** (2014) 090, doi:10.1007/JHEP06(2014)090, arXiv:1403.7366.
 167. ATLAS Collaboration, “Comprehensive measurements of t-channel single top-quark production cross sections at $\sqrt{s} = 7$ TeV with the ATLAS detector”, *Phys. Rev. D* **90** (2014), no. 11, 112006, doi:10.1103/PhysRevD.90.112006, arXiv:1406.7844.
 168. ATLAS Collaboration, “Evidence for the associated production of a W boson and a top quark in ATLAS at $\sqrt{s} = 7$ TeV”, *Phys. Lett. B* **716** (2012) 142, arXiv:1205.5764.
 169. CMS Collaboration, “Evidence for associated production of a single top quark and W boson in pp collisions at $\sqrt{s} = 7$ TeV”, *Phys. Rev. Lett.* **110** (2013) 022003, arXiv:1209.3489.
 170. CMS Collaboration, “Observation of the associated production of a single top quark and a W boson in pp collisions at $\sqrt(s) = 8$ TeV”, *Phys. Rev. Lett.* **112** (2014) 231802, doi:10.1103/PhysRevLett.112.231802, arXiv:1401.2942.
 171. CMS Collaboration, “Measurement of the ratio B(t to Wb)/B(t to Wq) in pp collisions at $\sqrt(s) = 8$ TeV”, *Phys. Lett. B* **736** (2014) 33, doi:10.1016/j.physletb.2014.06.076, arXiv:1404.2292.

172. DØ Collaboration, “Precision measurement of the ratio $B(t \rightarrow Wb)/B(t \rightarrow Wq)$ and Extraction of V_{tb} ”, *Phys. Rev. Lett.* **107** (2011) 121802, doi:10.1103/PhysRevLett.107.121802, arXiv:1106.5436.
173. CDF Collaboration, “Measurement of $R = B(tWb)/B(tWq)$ in top-quark-pair decays using lepton+jets events and the full CDF run II dataset”, *Phys. Rev. D* **87** (2013) 111101, doi:10.1103/PhysRevD.87.111101, arXiv:1303.6142.
174. CDF Collaboration, “Measurement of $R = \mathcal{B}(t \rightarrow Wb)/\mathcal{B}(t \rightarrow Wq)$ in Top–Quark–Pair Decays using Dilepton Events and the Full CDF Run II Data Set”, *Phys. Rev. Lett.* **112** (2014) 221801, doi:10.1103/PhysRevLett.112.221801, arXiv:1404.3392.